

Recent Progress in Electrolyte Development and Design Strategies for Next-Generation Potassium-Ion Batteries

Rakesh Verma,^[a] Pravin N. Didwal,^[a] Jang-Yeon Hwang,^[a] and Chan-Jin Park^{*[a]}

Rechargeable lithium-ion batteries (LIBs) have attained tremendous success and are extensively used in a wide range of fields. However, due to the scarcity and uneven geographical distribution of Li resources, its price is steadily increasing, which may limit its sustainable application in the near future. Potassium-ion batteries (PIBs) are promising alternatives to LIBs owing to the earth abundance, low cost, and eco-friendliness of potassium, and high energy density of PIBs. Although the field of PIBs has seen significant progress in the recent years, some challenges remain that limit their application, such as the severe side reactions between the electrolyte and electrodes, which result in an unstable solid electrolyte interphase, and thus, a

low coulombic efficiency. Hence, designing suitable electrolytes is necessary for the development of PIBs. This review summarises the current developments in PIB electrolytes and comprehensively discusses electrolyte design strategies for four major classes of electrolytes, namely non-aqueous, aqueous, ionic liquid, and solid-state electrolytes. In addition, the effects of the properties of each class of electrolyte are discussed in detail. Furthermore, ionic liquid electrolytes, an emerging class of electrolytes, are discussed in detail with respect to PIBs. Finally, several critical issues, challenges, and prospects of PIB electrolytes are discussed, and an outlook for the future research direction of PIBs is presented.

1. Introduction

Rechargeable lithium-ion batteries (LIBs) are widely used in mobile electronics and electric vehicles owing to their long lifespan and high energy density.^[1–4] However, the increasing cost of Li due to the scarcity and uneven geographical distribution of Li resources may limit its sustainable application in the near future.^[5,6] Consequently, next-generation secondary batteries based on earth-abundant elements, namely Na, K, and Mg, are considered promising alternatives to LIBs in future energy storage systems.^[7–15] Among them, potassium-ion batteries (PIBs) have recently attracted significant attention owing to their low cost, eco-friendliness, and high energy density.^[5,6,12] The physical and electrochemical properties and economic parameters of K-, Na-, and Li-ions are presented in Table 1.^[13,16–25] As shown in Table 1, the main advantages of PIBs are as follows: 1) PIBs are relatively inexpensive and environmentally friendly compared with LIBs as potassium (2.09 wt%) is more abundant and less toxic than lithium (0.0017 wt%) (Table 1); 2) PIBs exhibit a high cell potential and high energy density comparable to those of LIBs (Figure 1a), as the standard redox-potential of K^+/K (-2.93 V vs. SHE) is close to that of Li^+/Li (-3.04 V vs SHE) (Table 1); 3) the Stokes' radius of K-ion is smaller than those of Li- and Na-ions due to its weaker Lewis acidity than other ions (Figure 1b), which results

in a lower desolvation energy, higher ionic mobility, and higher transport number of the electrolyte;^[26] and 4) Al foil can be used as a current collector instead of Cu in anode part of PIBs because of the absence of an alloying reaction between potassium metal and Al foil, which can remarkably reduce the weight and price of the battery.^[6,27] Recently, the number of publications dealing with PIBs has increased (Figure 1c). Much effort has been devoted to understanding the electrochemistry of PIBs to enhance and achieve high capacity, cyclability, and rate capability via several strategies based on the design and growth of battery configurations, electrode, and electrolytes.^[28]

The three main components of a battery are cathode, anode, and electrolyte, whose properties significantly affect the specific capacity, cyclability, and rate performance of the battery. Over the last few years, PIB research has been focused on the development of cathodes and anodes, as they determine the gravimetric and volumetric energy densities of the system. However, the electrolyte also significantly affects the electrochemical performance of PIBs, such as specific capacity, rate capability, working potential, and safety.^[29] Since the performance of a cell is all the results of harmony among all the components including anode, cathode, and electrolyte, searching the suitable electrolyte which can be highly ionic-conductive and compatible with electrodes is needed. In addition, the energy production by PIBs is strongly influenced by parasitic side reactions, and thus depends on the type of electrolyte. Depending on the type of electrolytes, PIBs can exhibit different electrochemical performances.

Electrolytes play a critical role in establishing important properties of a battery system, including internal resistance, thermal stability, power density, energy density, and cycle life (Figure 1d).^[30] For instance, the ionic conductivity of an electrolyte significantly affects the internal resistance of the battery.^[30,31] A highly conductive electrolyte with fast ion

[a] Dr. R. Verma, P. N. Didwal, Prof. J.-Y. Hwang, Prof. C.-J. Park

Department of Materials Science and Engineering

Chonnam National University

77, Yongbong-ro, Buk-gu, Gwangju 61186, South Korea

Fax: (+82)-62-530-1699

E-mail: parkcj@jnu.ac.kr

An invited contribution to a joint Special Collection between – ChemElectroChem and Batteries & Supercaps dedicated to research Beyond Lithium-Ion Batteries

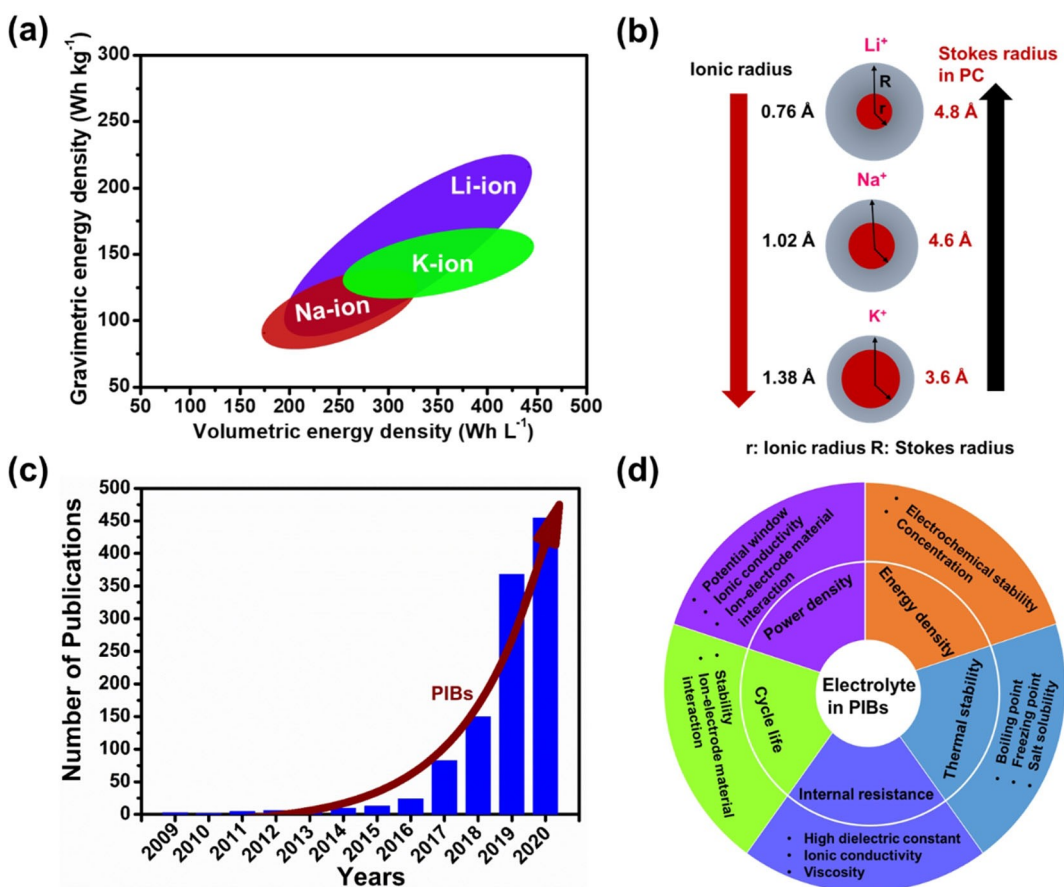


Figure 1. a) Comparison of energy densities of lithium-ion, sodium-ion, and potassium-ion batteries. b) Comparison of ionic radius and Stokes radius of lithium-ion, sodium-ion, and potassium-ion in PC. c) Number of publications on PIBs according to Web of Science (accessed December 31, 2020). d) Physical, chemical, and electrochemical effects of electrolyte on PIBs.



Dr. Rakesh Verma received his Ph.D. degree from Indian Institute of Technology Madras (IITM) in 2017. He has developed the ternary transition metal oxides and sulphides as new anode materials for rechargeable alkali Li/Na ion battery applications during his Ph.D. Currently, working as a postdoctoral research fellow in the Department of Materials Science and Engineering at Chonnam National University, South Korea. His current research work focused in the area of fabricating high-performance new anode materials for alkali metal ion (Li, Na, and K) batteries through innovative material designing and engineering.



Prof. Jang-Yeon Hwang received his Ph.D. degree (2018) on cathode materials for sodium-ion batteries at Hanyang University. He is currently an assistant professor in the Department of Materials Science and Engineering at Chonnam National University, Korea. His research is focused on the development of novel electrode materials for high-energy alkali-ion and alkali-metal batteries.



Pravin N. Didwal received his M.Sc. and M.Phil. degree from Department of Physics, Pune University, India. He is a Ph.D. candidate in Department of Materials Science and Engineering at Chonnam National University, South Korea. His research topic focuses on synthesis of nanomaterials and designing solid electrolyte for alkali metal ion batteries.



Prof. Chan-Jin Park is a professor of Materials Science and Engineering at Chonnam National University, Korea. He received his Ph.D. degree from Korea Advanced Institute of Science and Technology (KAIST) in 2003. From 2003 to 2005, he worked in POSCO Technical Research Lab. He joined the faculty of Department of Materials Science and Engineering at Chonnam National University in 2005. His research interests focus on the synthesis and characterisations of materials for rechargeable batteries including Li-ion, Na-ion, K-ion, Li-air, and Li-S batteries.

Table 1. Physical and electrochemical properties and economic parameters of potassium ion, sodium ion, and lithium ion.

| Properties | Li ⁺ | Na ⁺ | K ⁺ | Ref. |
|---|----------------------|-----------------|----------------|---------|
| Atomic mass [g mol ⁻¹] | 6.94 | 22.99 | 39.09 | [13] |
| Density [g cm ⁻³] | 0.53 | 0.97 | 0.86 | [13] |
| Melting point [°C] | 180.54 | 97.72 | 63.50 | [13] |
| Abundance [%] | 0.0017 | 2.36 | 2.09 | [16] |
| Distribution | 70% in South America | Everywhere | Everywhere | [17] |
| Potential vs. SHE [V] | -3.04 | -2.71 | -2.94 | [13,18] |
| Ionic radii [Å] | 0.76 | 1.02 | 1.38 | [19] |
| Stokes radii in PC [Å] | 4.8 | 4.6 | 3.6 | [20] |
| Stokes radii in water [Å] | 2.38 | 1.84 | 1.25 | [21] |
| Ionic conductivity of electrolyte of 1 M MFSI in PC [Scm ² mol ⁻¹] [M = Li, Na, and K] | 8.3 | 9.1 | 15.2 | [5] |
| Desolvation energy in PC [kJ mol ⁻¹] | 215.8 | 158.2 | 119.2 | [22] |
| Reaction potential of graphite vs. M/M ⁺ [V] [M = Li, Na, and K] | ~0.1 | ~0.7 | ~0.24 | [23] |
| Energy density of M ₂ C ₈ H ₄ O ₄ /PTCDA full cell [Wh/kg], [M = Li, Na, and K] | 131.1 | 164.1 | 147.3 | [24] |
| Cost of carbonate [USD ton ⁻¹] | 6,500 | 200 | 1,000 | [25] |
| Cost of industrial grade metal [USD ton ⁻¹] | 100,000 | 3,000 | 13,000 | [25] |

mobility and a high dielectric constant, low viscosity usually demonstrates an outstanding rate capability, which is beneficial for energy density as well as power density.^[32] In addition to ionic conductivity, the electrolyte potential window also considerably affects the power density and energy density of PIBs by enabling higher cell potential.^[30] To date, various electrolytes have been developed. Based on their physical properties, electrolytes are mainly classified as liquid and solid-state electrolytes (Figure 2).^[30] Liquid electrolytes are classified into aqueous and non-aqueous electrolytes, and non-aqueous electrolytes are further classified into organic and ionic liquid electrolytes. Solid-state electrolytes are categorised into quasi-solid and all-solid electrolytes, and quasi-solid electrolytes are further categorised into hydrogel polymer and organogel polymer electrolyte. In addition, the all-solid electrolyte can be classified into two main groups such as inorganic solid state and solid polymer electrolyte. Each electrolyte has its own benefits and disadvantage in PIBs applications.

In this review, we mainly focus on the progress in the development and design strategies of electrolytes for PIBs. We discuss four major classes of electrolytes, namely non-aqueous, aqueous, ionic liquid (IL), and solid-state electrolytes in terms of diagnosis and perspective. In addition, we also discuss a new class of IL electrolytes for PIBs in more detail. Moreover, we examine various approaches to improve the specific capacity, cycle life, and rate performance of PIBs. The purpose of this review is to explain the importance of electrolytes in PIBs and examine the potential of current and emerging electrolytes in the advancement of PIBs. Finally, we present future perspectives for rechargeable PIBs.

2. Non-Aqueous Liquid Electrolytes for PIBs

Non-aqueous liquid electrolytes are the most widely used electrolytes in LIBs, SIBs, and PIBs owing to their fascinating properties such as a higher ionic conductivity than that of solid

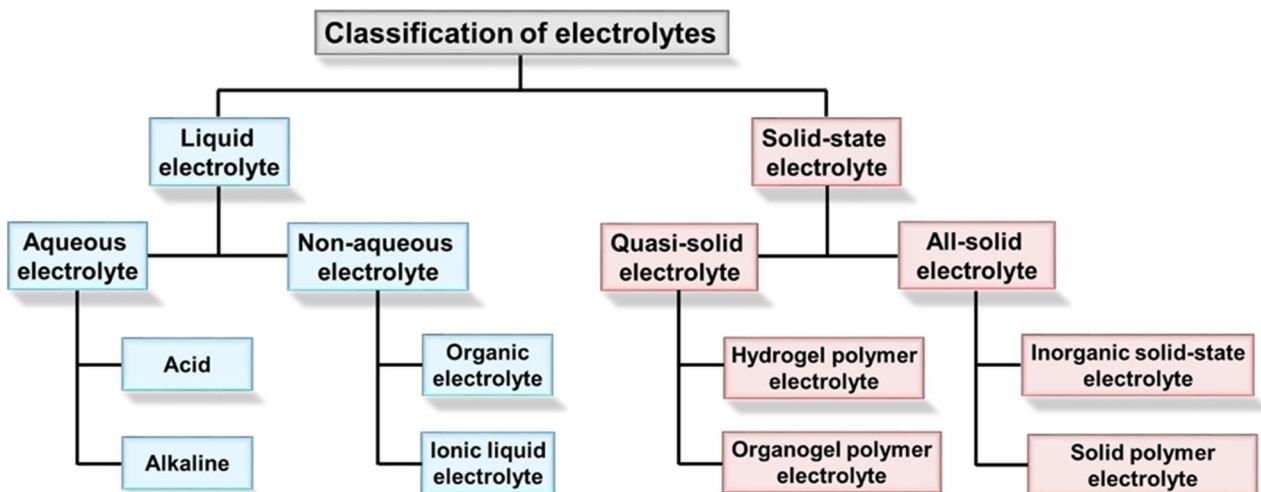


Figure 2. Classification of electrolytes for PIBs.

electrolytes, a wide potential window, and good compatibility with various electrode materials. Recently, our group developed a $\text{SnP}_3@\text{C}$ nanocomposite as an anode material and evaluated the electrochemical performance using 0.75 M KPF_6 in ethylene carbonate/diethyl carbonate (EC/DEC) as an electrolyte.^[12] The cell delivered an initial reversible capacity of 410 mAh g^{-1} , retained a specific capacity of 408 mAh g^{-1} over 50 cycles at 50 mA g^{-1} , and exhibited an excellent rate performance (Figure 3a).^[12] In addition, the authors proposed potassium alloying and dealloying mechanisms, as shown in Figure 3b.^[12] Furthermore, using the same electrolyte, we also tested mesoporous carbon (OPDMC-1000) as an anode material.^[6] The optimised OPDMC-1000 electrode exhibited impressive cycle life at high specific current of 500 mA g^{-1} and maintained a reversible specific capacity of 112 mAh g^{-1} over 3,000 cycles, which giving to a coulombic efficiency of almost 100% (Figure 3c).^[6] Nonetheless, the thermal stability, electrochemical stability, and safety still need to be improved for practical use in battery applications. To resolve these issues, a smart combination of novel potassium salts, new organic solvents, and additives have been designed for non-aqueous liquid electrolytes. Besides, various electrolyte additives, which are beneficial for stabilising the solid electrolyte interphase (SEI) layer, have been developed.^[33,34] In addition, in the recent years, significant efforts have been devoted to the development of highly concentrated organic electrolytes owing to their high oxidation resistance. This would be advantageous in electrolyte stability and improving the thermal stability, rate performance, and electrochemical potential range.^[35,36] Moreover, some highly concentrated electrolytes facilitate the formation of SEI on the

negative electrode and improve the current collector stability.^[37]

However, non-aqueous liquid electrolytes pose serious safety issues because of the flammability of organic solvents. Therefore, designing nonflammable concentrated electrolytes by replacing the highly flammable solvents is important for the commercialisation of these batteries. Recently, Liu et al. developed a nonflammable $(\text{CH}_3\text{O})_3\text{PO}$ (TMP) solvent that can resolve the safety issues of PIBs.^[38] The TMP solvent has several advantages such as fire retardance, wide temperature range between -46 to 197°C , low viscosity, and high dielectric constant. The optimised nonflammable concentrated electrolyte KFSI:TMP with a mole ratio of 3:8 was suitable for graphite electrodes. The graphite electrode maintained a high specific capacity of 279 mAh g^{-1} after 2,000 cycles at 0.2 C, and delivered a high coulombic efficiency (CE) of 99.6% (Figure 4a).^[38] The high cycling stability is attributed to the formation of a uniform stable F-rich SEI layer, which significantly inhibits electrolyte decomposition. The formation of a uniform SEI layer depends on the electrolyte salt composition. At an electrolyte having composition of salt to solvent ratio of 1:8 (KFSI:TEM), the K^+ cations were not fully solvated because of the solvation structure, which leads to serious solvent decomposition and irreversible capacity loss during the charging process. With an increase in mole ratio to 3:8 (KFSI:TEM), all the TEM molecules are fixed in the primary solvated shell of K^+ ions and generate a uniform stable SEI layer, as shown in Figure 4b.^[38] Further, the electrochemical performance of K-K symmetric cells using the optimised nonflammable electrode was studied, as shown in Figure 4c.^[38] The potassium metal in the nonflammable concentrated electrolyte resulted in stable

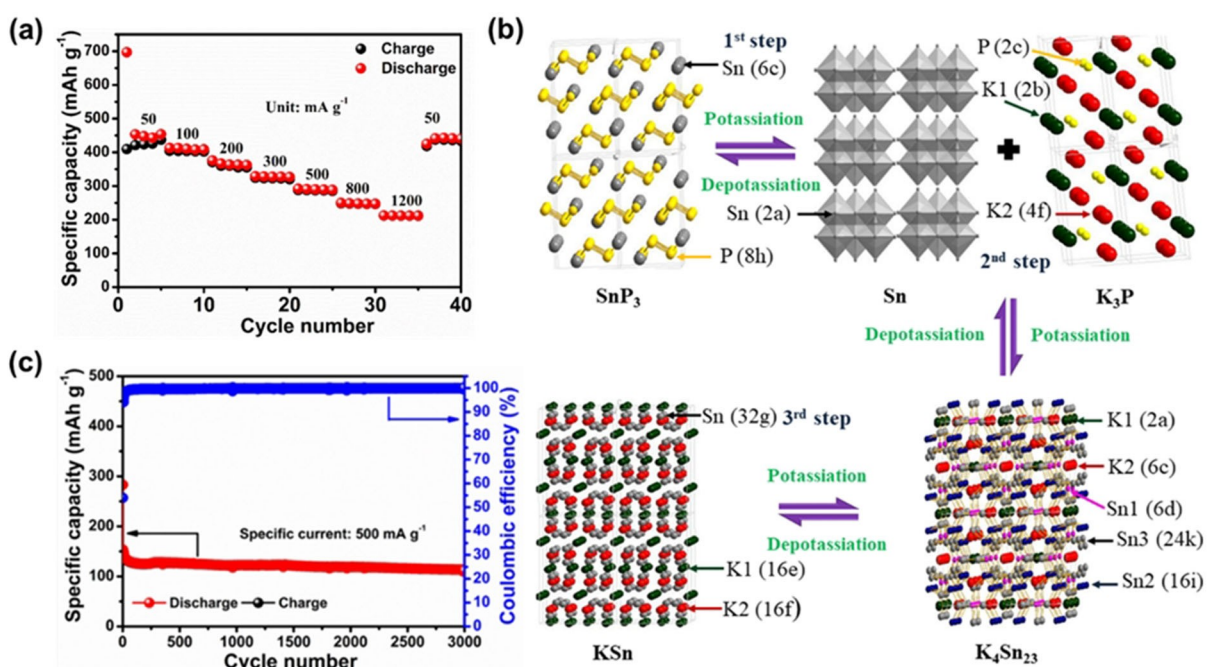


Figure 3. a) Rate performance of the SnP_3/C electrode obtained by varying the specific current from 50 to 1,200 mA g^{-1} and b) reaction mechanism of SnP_3/C nanocomposite electrode. Reproduced from Ref. [12] with permission. Copyright (2019) American Chemical Society. c) Cyclability of the optimised mesoporous carbon (OPDMC-1000) electrode at high specific current of 500 mA g^{-1} . Reproduced from Ref. [6] with permission. Copyright (2020) Wiley-VCH.

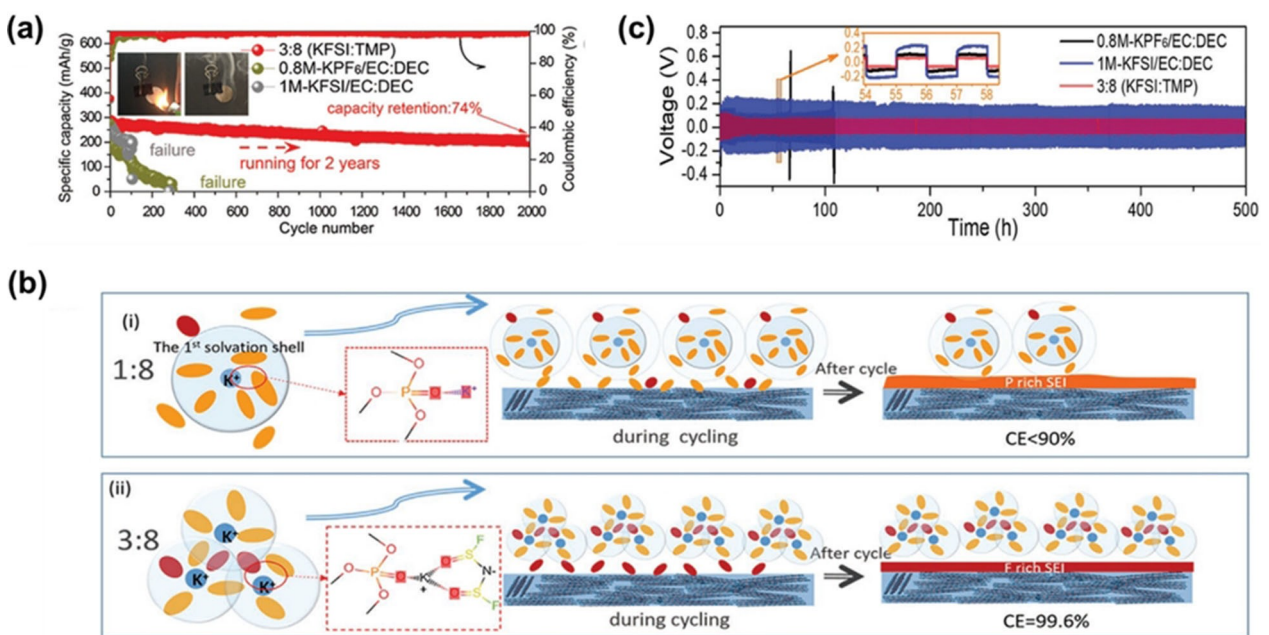


Figure 4. a) Long-term cycling performance of graphite electrode in various electrolytes. b) Schematic of solvation structure and SEI formation on graphite in (i) KFSI:TMP (1:8) electrolyte and (ii) KFSI:TMP (3:8) electrolyte. c) Cycling curves of K–K symmetric cells with different electrolytes at a current density of 1 mA cm⁻². Reproduced from Ref. [38] with permission. Copyright (2020) Wiley-VCH.

plating and stripping with a smaller polarisation cell potential of 0.12 V compared with the other electrolytes.

$$\sigma = \sum_i n_i \mu_i z_i e \quad (1)$$

3. Requirements and Design of Electrolytes

An appropriate electrolyte is the key factor in the realisation of PIBs with long cyclability, safety, and high energy density. In this section, we discuss the types of electrolytes that can satisfy the requirements for high-performance PIBs and the properties that need to be considered to select the appropriate electrolyte. In addition, we discuss the three main properties of electrolytes and explain their effects on the electrochemical performance of PIBs.

3.1. Transport Properties

Ionic conductivity is one of the important transport properties used to evaluate the performance of electrolytes in PIBs. Generally, aqueous electrolytes have a high ionic conductivity owing to the low viscosity of water and high solubility of salts in water. The ionic conductivity of organic liquid electrolytes is slightly lower than that of aqueous electrolytes because of the high viscosity of the solvents and poor or limited solubility of salts in organic solvents. The ionic conductivity of solid-state electrolytes is the lowest among all the electrolyte types. To increase the reaction rate on electrodes, the ionic conductivity of electrolyte needs to be improved. The ionic conductivity (σ) of electrolytes is related to the free ion number (n), ionic migration rate (m), and valence of the positive and negative charges (z) by the following equation:

The variable in Equation (1) depends on the lattice energy of the potassium salt, solvation effect, and migration of the solvated ions. Hence, all the components, including the solvents, potassium salts, and additives affect the ionic conductivity of an electrolyte.

3.1.1. Effect of Potassium Salt

Electrolyte salts affect the cycling stability and CE of anodes and cathodes. The commonly used potassium salts in PIB electrolytes are KPF₆, KClO₄, KBF₄, KTFSe, and KFSI. These salts (0.5 M) were dissolved in propylene carbonate (PC) solvent at RT.^[39] As shown in Figure 5a,^[39] white precipitates formed in the case of KClO₄ and KBF₄, indicating the low solubility of KClO₄ and KBF₄ in PC. The low solubility limits of these salts restrict their wide application in PIB electrolytes. In contrast, KPF₆, KTFSe, and KFSI formed clear solutions without precipitation, which indicate that the solubility of KPF₆, KTFSe, and KFSI in PC is higher than 0.5 M.^[5,40] As expected from the solubility results, the ionic conductivities of KPF₆, KTFSe, and KFSI electrolytes, ranging between 5.5 and 8 mS cm⁻¹, are much higher than those of KClO₄ and KBF₄ (Figure 5b).^[39] Hence, KPF₆, KTFSe, and KFSI are the preferred potassium salts for application in PIBs. Because KPF₆ is moderately soluble in carbonates, esters are mainly used as solvents in PIBs. This electrolyte usually has a low CE and high irreversible capacity due to the formation of an unstable SEI film on the electrode surface.^[6,12,41,42] Hence,

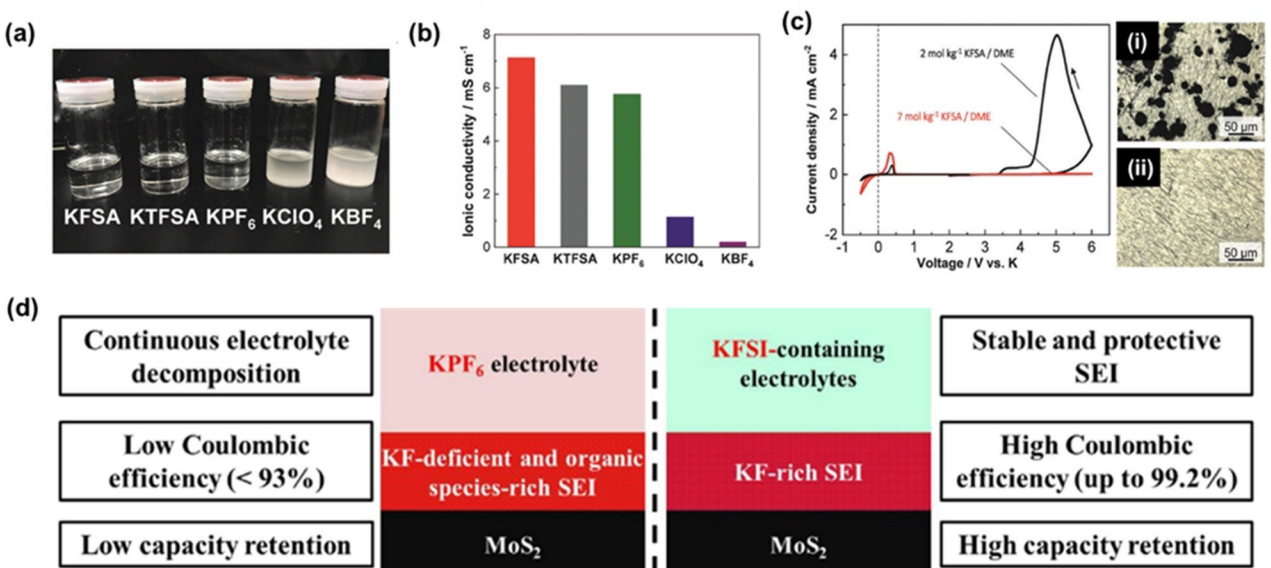


Figure 5. a) Photograph of solutions of KFSA, KTFSA, KPF₆, KBF₄, and KClO₄ in PC (concentration: 0.5 mol per dm³) after 12 h of stirring. b) Ionic conductivities of the prepared solutions at 25°C. c) Cyclic voltammograms of Al working electrodes in 2 mol kg⁻¹ and 7 mol kg⁻¹ of KFSA/DME solutions at a scan rate of 0.5 mV s⁻¹ in the voltage ranges of 2 to -0.5 V and 2 to 6 V in a K-Al cell. Optical microscopy images of Al working electrodes tested in (i) 2 mol kg⁻¹ KFSA/DME and (ii) 7 mol kg⁻¹ KFSA/DME after 3 cycles of CV in the voltage range of 2–6 V. Reproduced from Ref. [39] with permission. Copyright (2018) Royal Society of Chemistry. d) Effect of salt on MoS₂ electrode stabilisation of SEI layer. Reproduced from Ref. [33] with permission. Copyright (2019) American Chemical Society.

good electrolytes that can resolve the issues of electrolyte decomposition and passivation need to be urgently developed to realise high-performance PIBs.

Recently, imides based on novel potassium salts such as KFSI and KTFSI have been proposed as alternatives to traditional PIB electrolytes.^[43,44] Zhang et al. fabricated a battery with Sn₃P₃@C fibre electrode and KFSI in EC/DEC electrolyte and achieved a reversible capacity of 403.1 mAh g⁻¹ over 200 cycles at a specific current of 50 mA g⁻¹. Moreover, the symmetrical K-K battery exhibited stable cyclability over 100 cycles at a current density of 1 mA cm⁻². The result indicates that the KFSI electrolyte facilitated the formation of a uniform stable SEI film on the potassium metal anode surface and reduced polarisation. In addition, KFSI-based electrolytes can improve the specific capacity, cycle life, and rate performance of other electrode materials, namely carbonaceous materials, metal oxides, metal sulphides, and alloy-type materials.^[45] Furthermore, the electrochemical performance of a concentrated KFSI-EMC (1:2.5 mole ratio) was evaluated.^[46] The highly concentrated electrolyte facilitated the formation of a robust SEI layer on a graphite anode, resulting in a high area specific capacity of 7.36 mAh cm⁻², and enabled stable operation over 2,000 cycles without any capacity loss. However, highly concentrated electrolytes corrode the Al current collector at high potentials.^[47] Recently, Hosaka et al. addressed this issue by using a KFSI-DME electrolyte (7 mol/kg) that did not corrode the Al collector, as determined by cyclic voltammetry (CV) measurements (Figure 5c).^[39] Liu et al.^[48] also proposed a concentrated KTFSI-DME electrolyte and evaluated its performance with a V₂O₅ cathode. The V₂O₅ cathode delivered a reversible capacity of 93 mAh g⁻¹ at 50 mA g⁻¹. Even at a high

specific current of 500 mA g⁻¹, the cell exhibited 94% retention capacity after 200 cycles. The excellent performance was attributed to the high salt concentration, increased interaction between K⁺ and TFSI⁻, and a decrease in free solvent molecules in the electrolyte. Furthermore, better compatibility with the Al current collector is found with increasing electrolyte concentration.

Recently, electrolytes based on binary salts (KPF₆-KFSI) have been extensively developed. The cycling stability of a MoS₂ electrode significantly improved when a binary salt electrolyte was used instead of a single salt electrolyte.^[33] The reason for the significant improvement in the cycling stability of MoS₂ electrode using the binary salt electrode is summarised in Figure 5d.^[33] The formation of the stable, protective, and KF-rich SEI layer on the surface of the MoS₂ electrode contributed to improving the cycling stability. Hosaka et al. also developed a KPF₆-KFSI binary salt electrolyte.^[49] The optimised mole ratio of the binary salts was more than 3, and the electrolyte exhibited good antioxidant properties. Under the potential at 4.6 V, no obvious corrosion of the current collector was observed over 100 h. The binary salt electrolyte effectively inhibited Al corrosion. Furthermore, Zhang et al. prepared a Bi@rGO nanocomposite anode by a facile solution method and used it with various binary potassium salt electrolytes (KPF₆ and KFSI).^[50] They found that the SEI layer formed in the KFSI electrolyte was thinner than that formed in the KPF₆ electrolyte. In the KPF₆ electrolyte, the continuously forming SEI consumed the electrolyte constantly, and the thickness of the formed interface layer increased due to the pulverisation of Bi nanoparticles and the fragile SEI layer (Figure 6a).^[50] In contrast, the KFSI electrolyte led to the formation of a more robust and

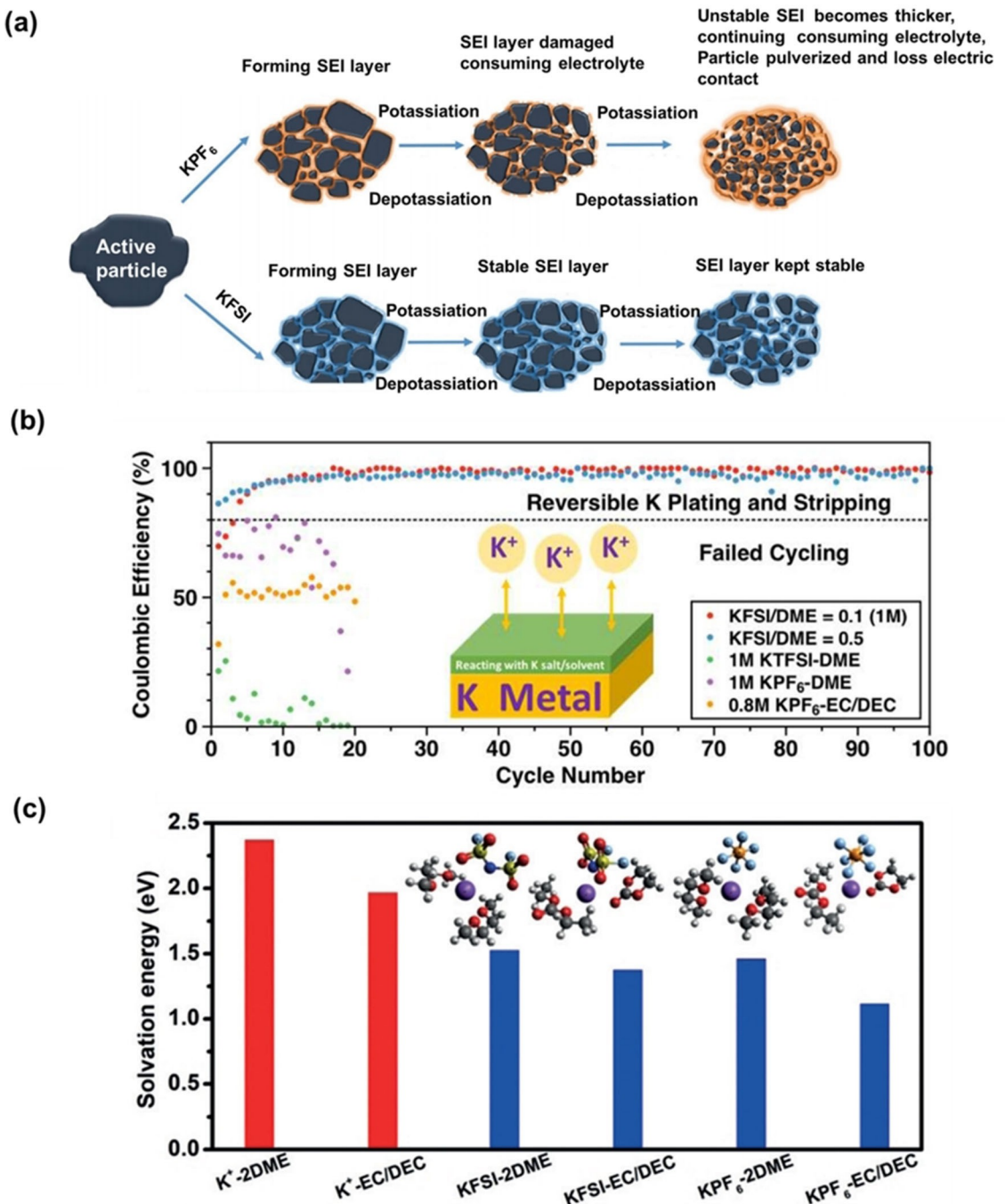


Figure 6. a) Schematic of the proposed stabilisation effects of an electrolyte on the SEI layer of a Bi/rGO electrode. Reproduced from Ref. [50] with permission. Copyright (2018) Wiley-VCH. b) Comparison of the cycling performance of potassium plating and stripping on a Cu substrate at a rate of 0.05 mA cm^{-2} . Reproduced from Ref. [51] with permission. Copyright (2017) American Chemical Society. c) Solvation energies in various electrolytes. Reproduced from Ref. [52] with permission. Copyright (2019) Wiley-VCH.

thinner SEI layer. The compositions of the SEI films formed in different potassium salt electrolytes were also investigated.^[5] The SEI layer formed in the KPF_6 electrolyte was mainly composed of organic components, which were mostly formed by the reduction of solvent. However, the SEI layer formed in the KFSI electrolyte was composed of inorganic/organic mixtures, which are the reduction products of the salts and solvent. Compared with organic components, inorganic com-

ponents have better mechanical strength and can thus adapt to large volume changes, and therefore form a more stable SEI.^[50,46]

Salts are considered to significantly affect the electrochemical performance of PIBs. Xiao et al. compared the performance of cells comprising different potassium salts in a DME solvent with that of a cell comprising an EC/DEC solvent by galvanostatic discharge/charge measurements.^[51] The cell

with the KFSI-DME electrolyte exhibited reversible K plating/stripping with an excellent efficiency of ~99% (Figure 6b),^[51] and the electrolyte exhibited high electrochemical stability up to 5 V vs. K/K⁺, which makes it compatible with high-potential cathodes. In contrast, the cells comprising 1 M KPF₆-DME, 1 M KTFSe-DME, and 0.8 M KPF₆-EC/DEC electrolytes exhibited rapid capacity decay and low CEs. The solvation energy of KFSI is higher than that of KPF₆ (Figure 6c).^[52] Hence, KFSI-based electrolytes contained more K⁺-solvated molecules, which significantly minimised the side reactions. We therefore conclude that compared with other potassium salt-based electrolytes, KFSI-based electrolytes are beneficial for the formation of uniform, robust SEI layers, resulting in a high specific capacity and excellent cyclability. In addition, compared with concentrated electrolytes, KFSI-based electrolytes have a lower viscosity and lower cost.

3.1.2. Effect of Solvent

A solvent is the second crucial component of electrolytes. The solvent should be stable, inexpensive, and nontoxic, and should have a high solubility for salts. Various types of solvents can satisfy these requirements in various ways, including organic solvents, ILs, and polymers. We summarise the recent advancements and current trends in electrolyte solvents to provide some direction for future research. In this section, we discuss the different types of solvents used on PIBs in the last few years, the required properties, and their advantages and disadvantages for PIB application.

Generally, an organic solvent is the main component of an electrolyte and significantly affects the electrolyte performance. An ideal electrolyte solvent must have a high dielectric constant (i.e., high polarity), low viscosity (η) to ensure a high ionic mobility, wide operating temperature range, high boiling point, low melting point, high flash point, low toxicity, and low cost, and must ensure the stability of electrode materials in a wide potential window during cell operation.^[53] Organic solvents are widely used in electrolytes for not only LIBs, but also next-generation batteries. Organic solvents used in electrolytes can be mainly categorised as organic esters (such as EC, PC, dimethyl carbonate (DMC), and DEC) and organic ethers (such as DME, glycoldimethyl ether, and DOL).

3.1.2.1. Ester Solvents

EC is the most common ester electrolyte used to increase the ionic conductivity by increasing the solubility of potassium salts, which effectively improves the CE and reversible specific capacity of PIBs.^[54] Pham et al. investigated the solvation energies of potassium, sodium, and lithium ions in EC by molecular dynamics simulations and found that the solvation structure of potassium ion is the smallest among the three.^[55] This indicates that the lower the desolvation energy, the faster is the ion transport in the electrolyte, which results in an excellent rate capability. Zhao et al. compared the cycling

stability of cells using three conventional ester electrolytes, EC/PC, EC/DEC, and EC/DMC, respectively.^[56] As demonstrated in Figure 7a and b,^[67] the CE decreased rapidly over 70 cycles in the EC/DMC electrolyte, indicating an unstable SEI layer growth, severe and continuous mass decomposition of DMC at low potentials, and poor cyclability of the reduction products.^[57–59] However, an excellent cycle life of more than 200 cycles with a high CE and high specific capacity was achieved with the EC/PC and EC/DEC electrolytes. Literature survey has revealed that EC/DEC is one of the extensively studied solvents. Although EC/DEC has a wide potential window,^[60] the stability of the SEI film depends on not only the activity of solvent, but also the stability of the reaction products. Thus, the stability of the anode–electrolyte interface needs to be studied in detail. Furthermore, a new type of ester electrolyte, triethyl phosphate (TEP), has been developed as an alternative to traditional ester electrolytes discussed above. Liu et al.^[61] proposed a KFSI-TEP electrolyte that facilitated the stable plating/stripping of the potassium metal anode with a high CE of 99.6% over 500 cycles with a small voltage hysteresis. Similarly, Deng et al.^[62] reported that a cell with a K_{0.5}MnO₂ cathode and KFSI-TEP electrolyte exhibited 84% capacity retention over 400 cycles and a CE of over 99.6%. Moreover, unlike in the case of traditional electrolytes (EC/DEC), the K_{0.5}MnO₂ cathode in the TEP electrolyte retained the original bulk structure during charge/discharge. Furthermore, the nonflammable electrolyte enhanced the safety of the battery. In contrast, a serious spalling and fracture phenomenon was observed in the case of EC/DEC electrolyte.

3.1.2.2. Ether Solvents

Generally, ethers exhibit higher solubility than traditional ester electrolytes.^[63] In addition, since ether-based electrolytes facilitate the formation of stable SEI films and significantly increase the CE, they are the preferred electrolytes for PIBs. In highly concentrated ether-based electrolytes, the ether molecules are tightly bound to the salt ions; thus, the stability of the system increases.^[64] DME as a common ether solvent has been extensively studied.^[35,39,51] Hosaka et al.^[39] reported that a graphite anode with highly concentrated KFSI-DME electrolyte results in an excellent ionic conductivity and facilitates the formation of a stable SEI film. The graphite anode delivered a CE of 99.3% and the graphite-K₂Mn[Fe(CN)₆] full cell exhibited a capacity retention of 85% after 101 cycles. Xiao et al. also applied a similar approach and evaluated the performance of a symmetric K–K cell and full cell comprising a highly concentrated (KFSI-DME) electrolyte. They found that compared with the dilute electrolyte, the highly concentrated electrolyte provided excellent oxidation durability. Recently, Zhang et al. fabricated various concentrations of KTFSe-DEGDME electrolyte and evaluated the cycling performance and rate capability of a Bi@C anode.^[65] The Bi@C electrode exhibited a superior cycle life after 600 cycles with 85% capacity retention. With increasing electrolyte concentration, the reduction current of the electrolyte decreased and the reversible capacity of the

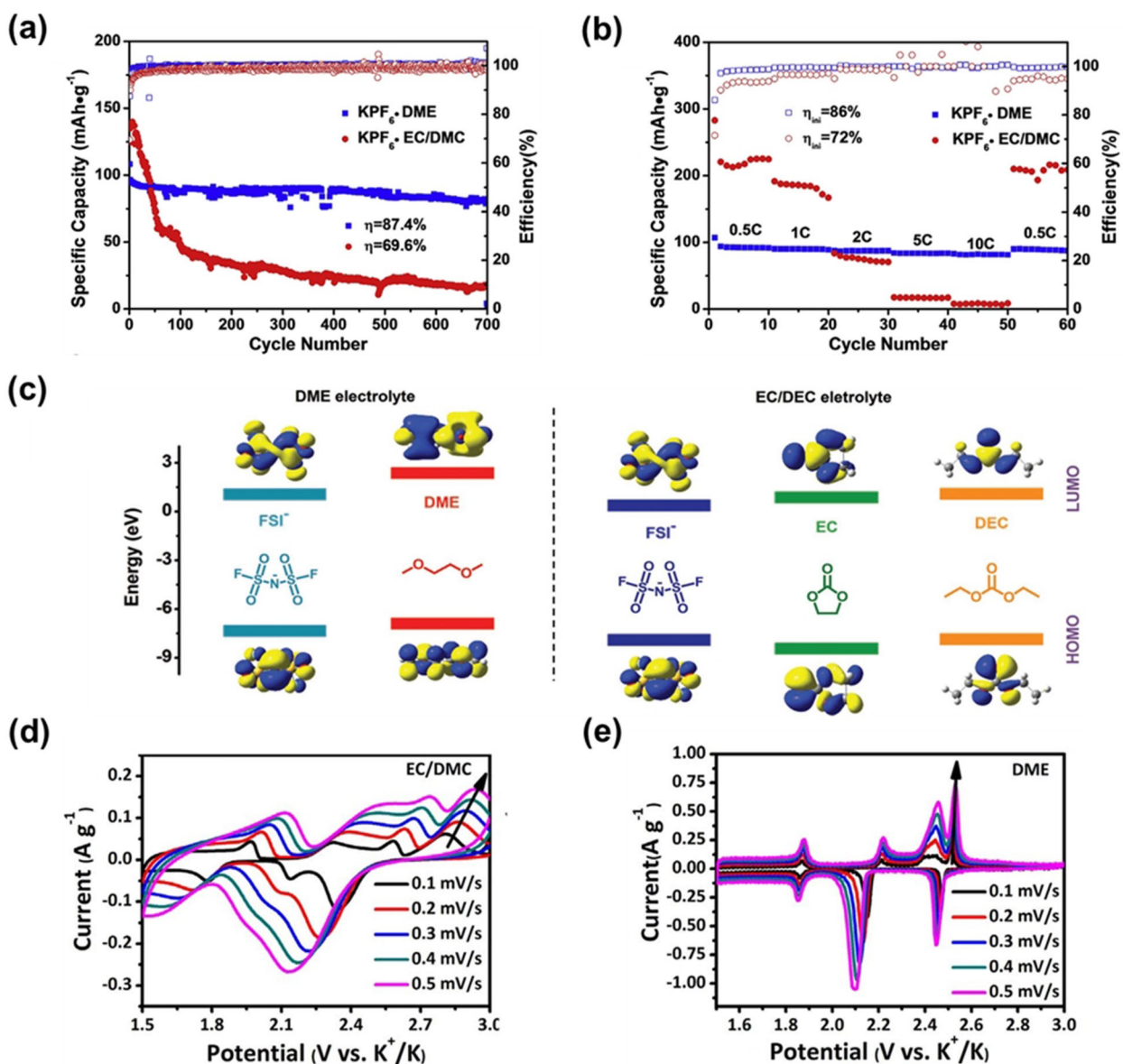


Figure 7. Electrochemical performance of graphite: a) galvanostatic discharge/charge potential curves; b) rate capability. Reproduced from Ref. [67] with permission. Copyright (2018) Elsevier. c) HOMO and LUMO energy levels of solvent molecules and potassium salts: FSI⁻ and DME in DME electrolyte; FSI⁻, EC, and DEC in EC/DEC electrolyte. Reproduced from Ref. [69] with permission. Copyright (2018) Wiley-VCH. Cyclic voltammograms of TiS₂; d) EC-DMC electrolyte, and e) DME electrolyte at scan rates of 0.1–0.5 mV·s⁻¹. Reproduced from Ref. [70] with permission. Copyright (2017) Elsevier.

Bi@C electrode increased. Xie et al.^[66] reported that highly concentrated ether-based electrolytes effectively suppress dendrite growth and form a uniform, stable SEI layer, thereby significantly enhancing the electrochemical performance of the battery.

Esters and ethers are the two main electrolyte solvents that have received significant attention for PIB applications (Table 2). The physical properties of solvent molecules significantly affect the electrolyte performance. The KFSI-DME electrolyte exhibits a low viscosity, high ionic conductivity, long cycle life, and excellent rate capability. Furthermore, SEI plays an important role in the cycling performance of PIBs. Wang et al. evaluated the electrochemical performance of a graphite anode used with ester and ether-based electrolytes.^[67] The graphite

anode with DME and EC/DMC electrolytes delivered initial CEs of 87.4% and 69.6%, respectively (Figure 7a and b).^[67] Moreover, a 3D N-doped SnSb nanocomposite was prepared by a solution method and its performance as a PIB anode was examined.^[68] The authors found that the interface resistance of DME-based electrolyte is lower than that of EC/DEC due to the formation of a uniform, stable SEI. Li et al. compared the electrochemical stability of DME and EC/DEC electrolytes and explained the SEI formation mechanisms.^[69] They determined the SEI formation mechanism from the highest occupied molecular orbital (HOMO) and lowest unoccupied molecular orbital (LUMO) of both the electrolyte salts and solvents evaluated by density functional theory calculations. As shown in Figure 7c,^[69] the LUMO energy level and reduction energy of

Table 2. Cyclability and initial coulombic efficiencies of PIBs composed of different electrolytes.

| Electrode materials | Electrolyte | Concentration [M] | Specific current [mA g^{-1}] | Initial CE [%] | Cycle number | Ref. |
|--|--------------------------|-------------------|---|----------------|--------------|-------|
| Fe ₃ C@PGC-NGF ^[a] | KPF ₆ -EC:DEC | 1.0 | 1,000 | 73 | 10,000 | [122] |
| APC-700 ^[a] | KPF ₆ -EC:DEC | 0.8 | 50 | 61.3 | 10,000 | [123] |
| NCNF-800 ^[a] | KPF ₆ -EC:DMC | 1.0 | 5,000 | 69.7 | 1,000 | [124] |
| N/S-doped carbon | KPF ₆ -EC:DEC | 0.8 | 100 | 50 | 200 | [125] |
| Graphite | KPF ₆ -EC:PC | 1.0 | 20 | 66.5 | 200 | [56] |
| | KPF ₆ -EC:DEC | 1.0 | 20 | 47.0 | 200 | |
| | KPF ₆ -EC:DMC | 1.0 | 20 | 42.7 | 200 | |
| Bi@rGO | KPF ₆ -EC:DEC | 0.8 | 50 | 47 | 50 | [50] |
| | KFSI-EC:DEC | 0.8 | 50 | 63 | 50 | |
| SPCS ^[a] | KPF ₆ -EC:DEC | 0.8 | 200 | 50.4 | 100 | [126] |
| | KFSI-EC:DEC | 1.0 | 200 | 34 | 100 | |
| | KPF ₆ -EC:PC | 0.8 | 200 | 51.6 | 100 | |
| | KFSI-DEM | 1.0 | 200 | 68.2 | 100 | |
| Sn ₄ P ₃ @C fibre | KPF ₆ -EC:DEC | 0.8 | 50 | 46.14 | 200 | [43] |
| | KFSI-EC:DEC | 0.8 | 50 | 64.17 | 200 | |
| Poly(antraquinonyl sulfide) | KTFSI-DOL:DME | 0.5 | 20 | 90 | 50 | [87] |
| Graphite | KPF ₆ -EC:DMC | 1.0 | 2,800 | 69.6 | 700 | [67] |
| | KPF ₆ -DME | 1.0 | 2,800 | 87.4 | 700 | |
| 3D SnSb@NC | KPF ₆ -EC:DEC | 0.8 | 500 | 26.7 | 200 | [68] |
| | KPF ₆ -DME | 0.5 | 500 | 90.1 | 200 | |
| E-carbon | KPF ₆ -EC:EMC | 0.8 | 100 mA g^{-1} | 49.8 | ~500 | [121] |
| | KFSI-DME | 3.0 | 500 mA g^{-1} | 58.5 | 3,000 | |

[a] PGC: porous graphite carbon; NGF: N-doped graphenic framework; APC: argon porous carbon; NCNF: N-doped carbon nanofiber; SPCS: carbon spheres with nano-size and porous structure.

KFSI are lower than those of DME. Moreover, the reduction product of FSI⁻ was an inorganic compound, which formed a denser inorganic SEI layer. In contrast, the lower LUMO energy level of EC/DEC led to severe decomposition and side reactions, resulting in a thicker organic–inorganic SEI film. In addition, they found that the kinetics of ester and ether electrolytes were also different. Further, Wang et al.^[70] evaluated KPF₆ in DME and EC/DEC by CV. The CV results (Figure 7d and e)^[70] confirm that the linear molecular DME had a higher electron number and the Stokes' radius of potassium ion in DME was smaller than that of the potassium ion in EC/DEC, which resulted in a better kinetic performance. Therefore, ether-based electrolytes improve the cycle life and rate capability owing to their superior thermodynamic stability and better kinetics.^[67] Nevertheless, the SEI formation mechanisms in different solvents remain unclear and require further investigation. Further, ether solvents exhibit a weak antioxidant property that renders ether-based electrolytes unsuitable for high-potential full cell applications.^[50] Hence, improving the high-potential stability should be the future research direction in this field. Currently, ILs and polymers are the emerging classes of electrolytes for PIB application.

3.1.3. Effect of Additives

The additive is the third important component of a functional electrolyte and can significantly improve the cycling performance of LIBs and SIBs. Fluoroethylene carbonate (FEC) is a widely studied additive;^[71,72] the effect of FEC on K-ion electrolytes has been recently investigated. Most studies have concluded that FEC-based electrolytes are more suitable to cathodes at high potentials in PIBs.^[73,74] Bie et al. first studied

the effect of FEC on a K_{1.75}Mn[Fe(CN)₆]_{0.93}·0.16H₂O cathode. The addition of 2 vol% FEC to 0.7 M KPF₆ in an EC/DEC electrolyte increased the initial CE of the K_{1.75}Mn[Fe(CN)₆]_{0.93}·0.16H₂O cathode from 61% to 90%. He et al. also reported that the addition of 5% FEC to an EC/DEC electrolyte increased the CE of a K₂Fe[Fe(CN)₆] cathode to 98%. These studies revealed that the increase in CE by the addition of FEC to the electrolyte is attributed to the formation of a stable cathode/electrolyte interphase, which efficiently prevents further side reactions.

Further, Zhang et al. investigated the effect of FEC additive in an electrolyte on GeP₅ anode half cells.^[44] They observed that the solvation energy of the electrolytes without FEC (0.305 eV) was smaller than that of the electrolyte with FEC (1.28 eV) in PIBs (Figure 8a),^[44] this implies that the diffusion and desolvation of potassium ions into the electrolyte occurs easily. The FEC additive in PIBs deteriorates the specific capacity, cyclability, and rate performance (Figure 8b and c).^[44] Similarly, in another study,^[43] the specific capacity of a Sn₄P₃@carbon fibre anode significantly decreased after a few cycles when the electrolyte contained FEC (Figure 8d).^[43] They reported that FEC causes severe polarisation cell potential, due to this poor of the interface, thereby reducing the cycling stability of the anode at lower potentials. These results indicate that the effect of FEC on PIBs is different from its effect on LIBs and SIBs.^[75]

3.2. Electrochemical Stability

Electrochemical stability is directly related to the cycle life and safety of the batteries. The electrochemical stability window represents the electrode potential range in which the electrolyte is neither oxidised nor reduced. Hence, the electrochemical stability is governed by the oxidation/reduction potentials and

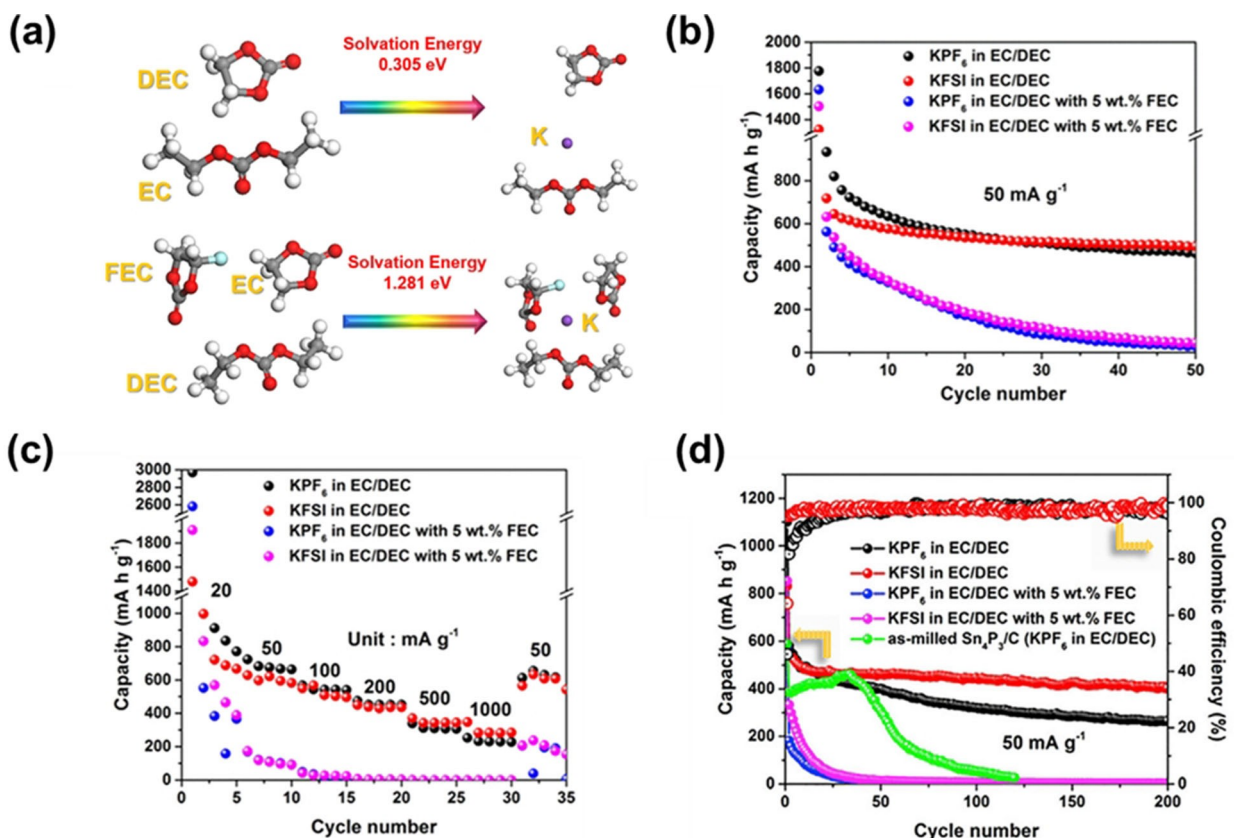


Figure 8. a) Solvation energies calculated from the binding energy of the K⁺ (Y) clusters, where Y = EC + DEC or EC + DEC + FEC. b) Cycle life and c) rate performance of GeP₅ electrode. Reproduced from Ref. [44] with permission. Copyright (2018) Elsevier. d) Cyclability of Sn₄P₃ electrode in various electrolytes at 50 mA g⁻¹. Reproduced from Ref. [43] with permission. Copyright (2018) Elsevier.

the Fermi level of the electrons in a solution.^[76] The energy states (HOMO and LUMO) of the electrode and electrolyte are presented in Figure 9a.^[76] The electrochemical stability of electrolytes is generally analysed by LSV. Recently, Chen et al. found that the electrochemical potential stability window directly depends on electrolyte concentration. At a high concentration of KFSI salt, a high potential stability window of 3.97 V was obtained, with cathode and anode limit potentials of -1.55 and 2.42 vs. Hg/Hg₂Cl₂, respectively (Figure 9b).^[83] Similarly, Jiang et al. demonstrated that the potential stability increased with increasing electrolyte concentration (Figure 10c).^[88] Furthermore, electrolyte composition, that is, the mixing of two different solvents and salts also affects the electrochemical potential stability window.^[77,78,5]

3.3. Thermal Stability

Organic liquid electrolytes tend to decompose during the charge/discharge process due to heat release and an increase in working temperature. The increase in temperature may pose safety issues for PIBs. Thus, the thermal stability of PIB electrolytes is an important factor in the commercialisation of PIBs. There are two aspects to the thermal stability of electrolytes: the electrolyte is thermally stable, or the electrolyte and electrode are thermally stable during their interaction in PIBs.

The thermal stability of an electrolyte is mainly studied by optimising the contents of solvent, salt, and additive.^[77,78] Most of the studies have been conducted at RT, and the effect of operating temperature on PIBs has not yet been investigated. The operating temperature plays a vital role in the LIB performance, particularly the cycle life and safety.^[79] Recently, Adams et al. conducted a novel study on the effect of a wide operating temperature range of 0–40°C on the cycling performance of a graphite anode in PIBs^[80] focusing on three parameters: kinetics and rate performance, polarisation, and cell aging. They observed fast kinetics at low temperatures and attributed it to an increase in charge-transfer resistance and solid-state diffusion activation energy. The graphite electrode exhibited an excellent cycle life at 40°C (Figure 9c).^[80] With an increase in temperature, capacity degradation occurred rapidly due to continuous SEI growth and an increase in charge-transfer resistance.

4. Aqueous Liquid Electrolytes for PIBs

Aqueous electrolyte-based PIBs are considered potential candidates for grid-scale applications because of the non-flammability and low cost of aqueous electrolytes compared with organic liquid electrolytes. In addition, the earth abundance, air stability, and high conductivity of potassium render the

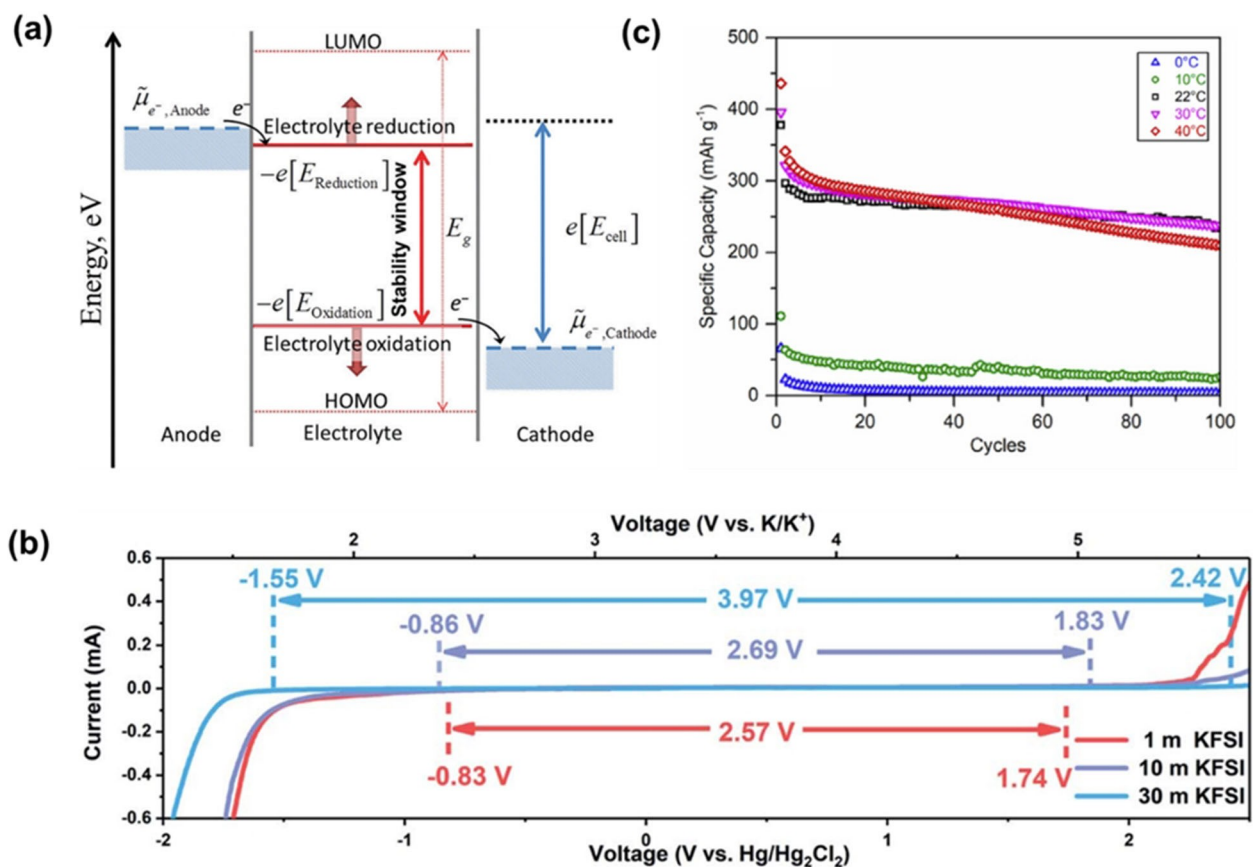


Figure 9. a) Electrolyte stability and HOMO and LUMO energy levels. Reproduced from Ref. [76] with permission. Copyright (2018) Royal Chemical Society. b) Linear voltammetry curves measured at 10 mV s^{-1} in 1, 10, and 30 M KFSI electrolyte. Reproduced from Ref. [83] with permission. Copyright (2020) Royal Society of Chemistry. c) Cycling performance of a graphite anode at 50 mA g^{-1} measured at different operating temperatures. Reproduced from Ref. [80] with permission. Copyright (2018) Elsevier.

aqueous PIBs an attractive technology. Considerable research has been conducted on aqueous electrolyte-based zinc-ion batteries (ZIBs), lithium-ion batteries (LIBs), and sodium-ion batteries (SIBs).^[81] Water is well known as the universal solvent because it dissolves more substances than any other liquid. In addition, the water emerges as a natural replacement for the organic solvents, it has a non-flammable, high dielectric constant (78 at 25°C), high dipole moment (1.8546 Debye), high acceptor (54.8), and donor number (18). Aqueous electrolytes are generally classified as conventional aqueous electrolytes such as KOH, KCl, K_2SO_4 and KNO_3 salt solutions, and water-in-salt electrolytes such as $\text{CH}_3\text{CO}_2\text{K}$ and $\text{CF}_3\text{SO}_3\text{K}$. The compatibility of organic materials with aqueous electrolytes makes them the appropriate choice for aqueous PIBs. Most organic electrode materials are soluble in organic electrolytes; hence, aqueous electrolytes are good alternatives to organic liquid electrolytes. However, to date, only a few organic materials have been reported for aqueous PIBs, and mostly carbonyl compounds have been used as anode materials.^[82–86]

Organic cathode and anode materials are more suitable for aqueous electrolytes and exhibit excellent K-storage performance because of a high K-ion conductivity and poor solubility in aqueous electrolytes.^[83,87] For instance, Li et al. used poly (anthraquinonyl sulphide) as a cathode material with an

aqueous 1 M KOH electrolyte for aqueous PIBs^[87] and achieved a large specific capacity of 128 mAh g^{-1} at specific current 2 A g^{-1} , which is higher than that (106 mAh g^{-1}) obtained with an organic electrolyte (0.5 M KTFSI in dioxane (DOL) and dimethyl ether (DME)) at the same specific current. Additionally, a high concentration of aqueous electrolyte further improved the capacity. Liang et al.^[82] assembled a full cell with a poly (anthraquinonyl sulphide) anode, Ni(OH)_2 cathode, and 10 M KOH electrolyte. The PAQS- Ni(OH)_2 full cell delivered an enhanced specific capacity of 186 mAh g^{-1} at a specific current 2 A g^{-1} .

Generally, the electrochemical stability potential window of conventional aqueous electrolytes is narrower (1.23 V) than that of organic electrolytes. Outside this potential window, water splitting occurs, resulting in the evolution of oxygen and hydrogen. The low utilisation of electrodes, together with a low operating cell potential, lowers practical energy density and thus hinders the application of aqueous PIBs in commercial batteries. To resolve this issue, water-in-salt concept-based electrolytes have been developed. Water-in-salt-based electrolytes offer various advantages such as a broad electrochemical potential window due to a low content of free water molecules, and a reduction in the dissolution of organic cathodes and anodes at high electrolyte concentrations. Currently, $\text{CH}_3\text{CO}_2\text{K}$

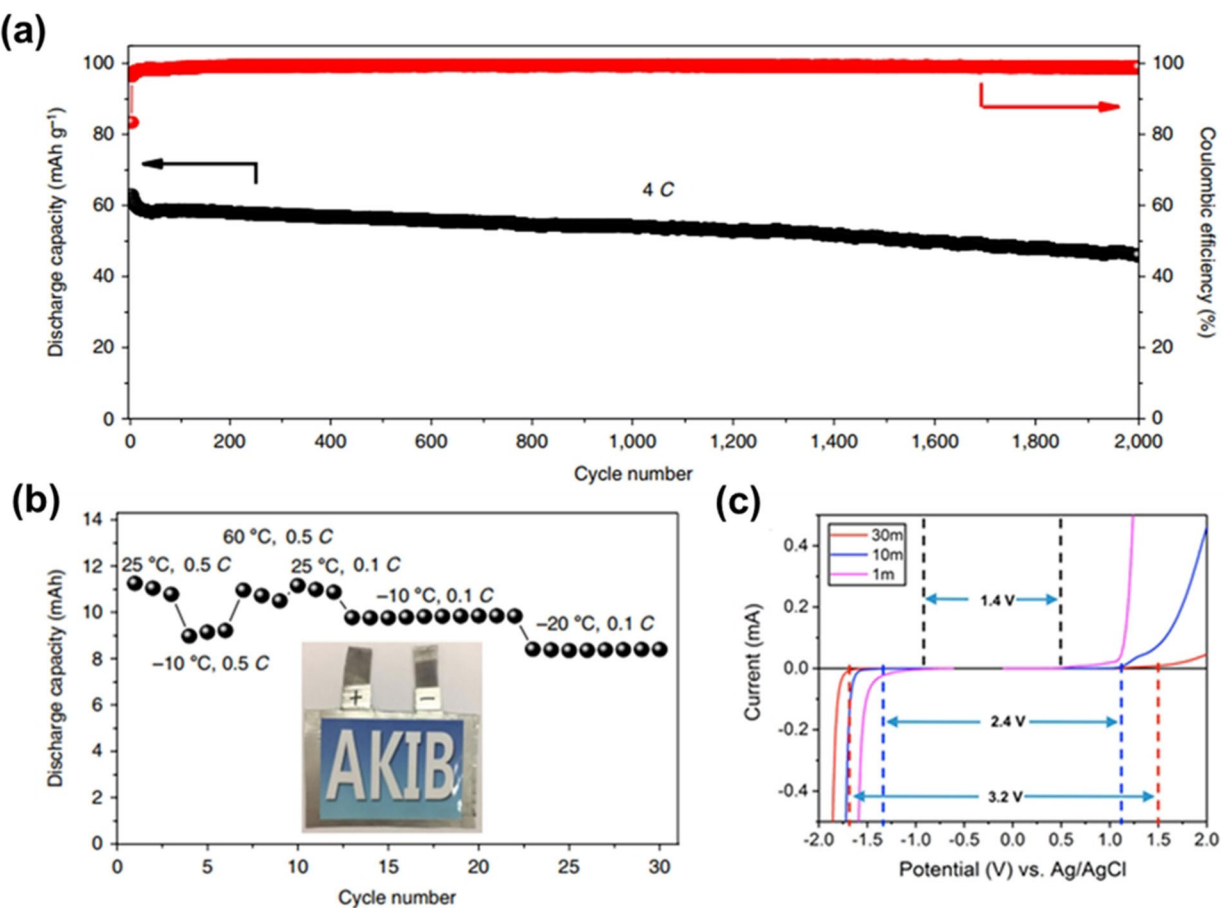


Figure 10. a) Cyclability and b) rate performance of the PTCDI/22 M $\text{KCF}_3\text{SO}_3/\text{KFeMnHCF-3565}$ pouch cell at different rates (0.5 and 0.1 C) and temperatures (-20 , -10 , 25 , and 60°C) within a cell potential range of 0 – 2.3 V. Reproduced from Ref. [84] with permission. Copyright (2019) Springer Nature. c) Linear voltammetry curves measured at 1 mVs^{-1} in 1 , 10 , and 30 M potassium acetate electrolytes. Reproduced from Ref. [88] with permission. Copyright (2018) American Chemical Society.

based salts have been used for water-in-salt electrolytes, exhibiting a higher potential range, compatibility with less expensive and abundant Al current collectors, and eco-friendliness.^[88] Leonard et al. also developed a highly concentrated (30 M) $\text{CH}_3\text{CO}_2\text{K}$ -based water-in-salt electrolyte that exhibited a high potential window of 3.2 V (Figure 10c).^[88] The results indicated that the aqueous 30 M $\text{CH}_3\text{CO}_2\text{K}$ electrolyte could increase the conductivity of LiTFSI and other similar fluorinated imide salts. However, the instability of aqueous PIBs in alkaline environments, such as that provided by the $\text{CH}_3\text{CO}_2\text{K}$ -based water-in-salt electrolyte, remains an obstacle in the utilisation of aqueous PIBs. Recently, Jiang et al. prepared a highly concentrated (22 M) KCF_3SO_3 water-in-salt electrolyte and examined its effect on the full cell performance.^[84] The concentrated electrolyte significantly reduced the dissolution of organic electrode materials because of a low content of free water molecules, and the full cell exhibited an excellent cycle life with a capacity retention of 73 % after 2,000 cycle at 4 C, a high energy density of 80 Wh kg^{-1} (Figure 10a),^[84] and good rate capability at a high rate (20 C) over a wide temperature range of -20 to 60°C (Figure 10b).^[84] In addition, some cathode materials were investigated for $\text{CH}_3\text{CO}_2\text{K}$ -based water-in-salt

electrolytes. The cathode materials exhibited excellent electrochemical properties owing to their high stability in water and a unique open crystal structure in neutral solutions used as the electrolyte (e.g., K_2SO_4 , KCF_3SO_3). However, the water-in-salt electrolyte are generally slightly costly than conventional aqueous electrolytes. Therefore, low-cost, highly stable aqueous electrolytes with a large potential window need to be urgently developed for application in aqueous PIBs.

5. Ionic Liquid (IL) Electrolytes for PIBs

ILs consist of inorganic or organic anions and organic cations and offer many advantages over aqueous and non-aqueous electrolytes such as a low vapour pressure, high-temperature stability, large operating potential window, low volatility, and low flammability. These unique physicochemical and electrochemical properties of ILs make them a promising candidate for electrolytes. Compared with non-aqueous electrolytes, ILs exhibit a better electrochemical performance and fewer safety issues for application in PIBs. In addition, potassium based ILs are beneficial in terms of stability against potassium metal.

Until now, only a few studies have been conducted on PIBs using ILs as electrolytes. The commonly used IL cations are imidazolium (e.g., $[\text{EMIM}]^+$), pyrrolidinium (e.g., PYR14), ammonium (e.g., $[\text{DEME}]^+$), and sulfonium (e.g., $[\text{Me}_3\text{S}]^+$), whereas the typically employed IL anions are tetrafluoroborate (BF_4^-), bis(trifluoromethanesulfonyl)imide (TFSI $^-$), and bis (fluorosulfonyl)imide (FSI $^-$). IL electrolytes based on potassium bis(trifluoromethanesulfonyl) amide (PTFSA) has been reported for high-voltage PIBs.^[89] Because these electrolytes can operate up to a potential of around 6.0 V, they can be safely used at high voltages. The physicochemical properties of KTFSA-based ILs are presented in Figure 11.^[89] Using the same electrolyte, Masese et al. assembled a cell and evaluated the cyclic performance and rate capability of honeycomb-structured layered $\text{K}_2\text{Ni}_2\text{TeO}_6$ and P2-type $\text{K}_{2/3}\text{Ni}_{1/3}\text{Co}_{1/3}\text{Te}_{1/3}\text{O}_2$.^[90] The layered cathode materials in IL exhibited a stable charge-discharge cycles even up to a high potential of 4 V vs. K/K^+ . Yamamoto et al. developed a new binary IL, $\text{K}[\text{N}(\text{SO}_2\text{F})_2]\text{-}[N\text{-methyl-N-propylpyrrolidinium}][\text{N}(\text{SO}_2\text{F})_2]$, for PIBs and evaluated its physicochemical and electrochemical properties.^[91] The binary IL electrolyte displayed a higher ionic conductivity (4.8 mS cm $^{-1}$ at 25 °C) than those of sodium and lithium-based ILs. Further, electrochemical characterisation revealed that potassium deposition and dissolution occurred at a more negative potential than that in the case of lithium and sodium metals, indicating that potassium-based ILs can provide a wider working potential window for PIBs. Further, Onuma et al. fabricated a full cell with a graphite anode, $\text{K}_2\text{Mn}[\text{Fe}(\text{CN})_6]$ cathode, and the same new binary IL electrolyte.^[92] The graphite- $\text{K}_2\text{Mn}[\text{Fe}(\text{CN})_6]$ full cell

displayed stable charge and discharge capacities over 200 cycle at room temperature (RT). Arnaiz et al. proposed an aprotic IL (1-butyl-1-methylpyrrolidinium bis(trifluoromethanesulfonyl) imide [Pyr₁₄TFSI]) and a protic IL (1-butylpyrrolidinium bis (trifluoromethanesulfonyl)imide [Pyr_{H4}TFSI]) as electrolytes for PIBs.^[93] The physicochemical properties such as viscosity and ionic conductivity of the ILs in PIBs are slightly higher than those reported for SIBs and LIBs. The electrochemical performance was examined by combining olive pit-derived hard carbon with the aprotic and protic IL electrolytes at RT and 60 °C. Souza et al. conducted molecular dynamics simulations of 1-ethyl-3-methyl imidazolium tetracyanoborate ($[\text{EMIM}]^+[\text{B}(\text{CN})_4]^-$) IL to determine the effect of $\text{Na}^+/\text{K}^+[\text{B}(\text{CN})_4]^-$ salts and polyethylene oxide (PEO) on transport mechanism,^[94] and reported that the IL mixture is a promising electrolyte for both SIBs and PIBs.

Recently, Yamamoto et al. used a pyrrolidinium-based IL, $\text{K}[\text{FSA-}[\text{C3C1pyrr}]\text{-FSA}]$, in a half cell based on Sn alloy anode^[95] and achieved first discharge and charge capacities of 328 and 167 mAh g $^{-1}$, respectively. Moreover, the cell maintained a high capacity of 173 mAh g $^{-1}$ after 100 cycles at RT. Sun et al. recently developed an IL electrolyte comprising 1-ethyl-3-methylimidazolium chloride/ AlCl_3/KCl /potassium bis (fluorosulfonyl) imide for safe and high-performance potassium metal batteries.^[96] The electrolyte is nonflammable (Figure 12b)^[96] and exhibits an ionic conductivity of 13.1 mS cm $^{-1}$ at RT, which is higher than those of organic and IL electrolytes (Figure 12a).^[96] The cell assembled using a potassium metal anode and ($\text{K}_{1.90}\text{Mn}_{0.92}\text{Co}_{0.08}[\text{Fe}(\text{CN})_6]_{0.96}$ @rGO) cathode exhib-

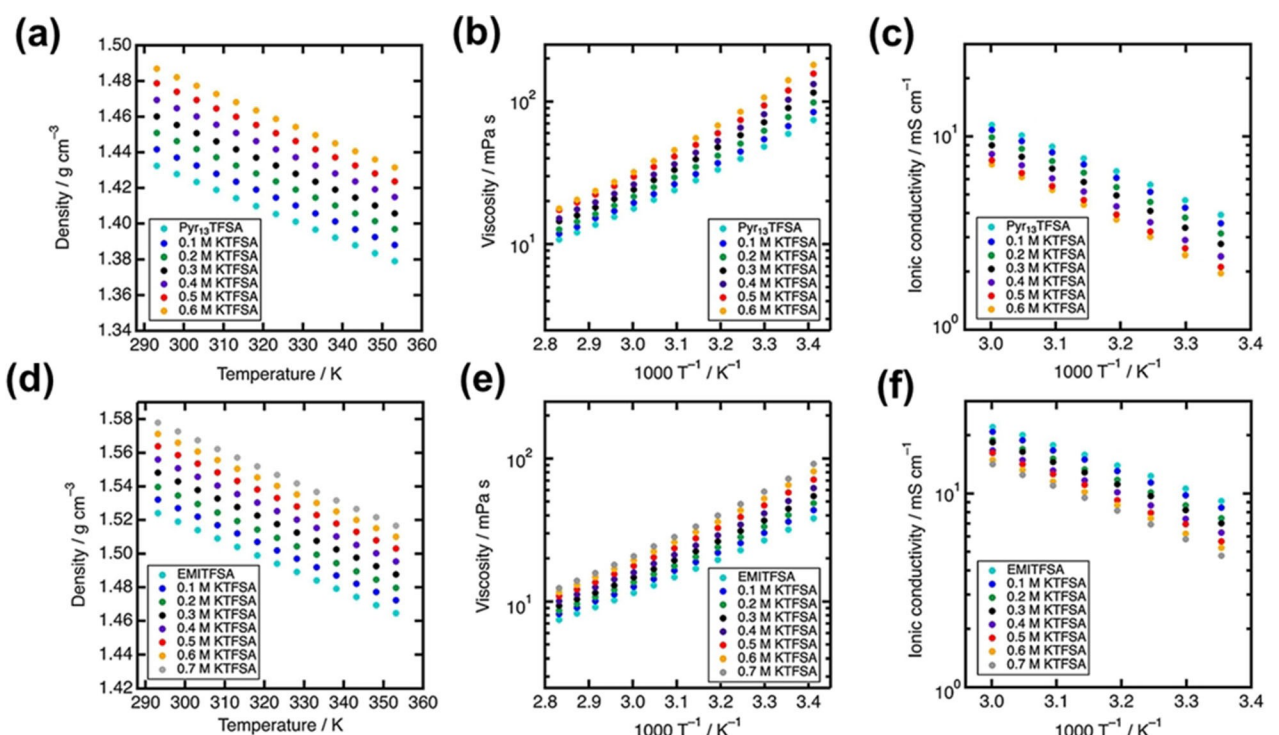


Figure 11. Physicochemical properties of potassium bis(trifluoromethanesulfonyl)amide (KTFSA)-based ionic liquids. Plots show the temperature dependence of a, d) density, b, e) viscosity, and c, f) ionic conductivity for KTFSA-based ILs using 1-methyl-1-propylpyrrolidinium TFSA (Pyr₁₃TFSA) and 1-ethyl-3-methyl imidazolium TFSA (EMITFDA) with various KTFSA salt concentrations. Reproduced from Ref. [89] with permission. Copyright (2019) Wiley-VCH.

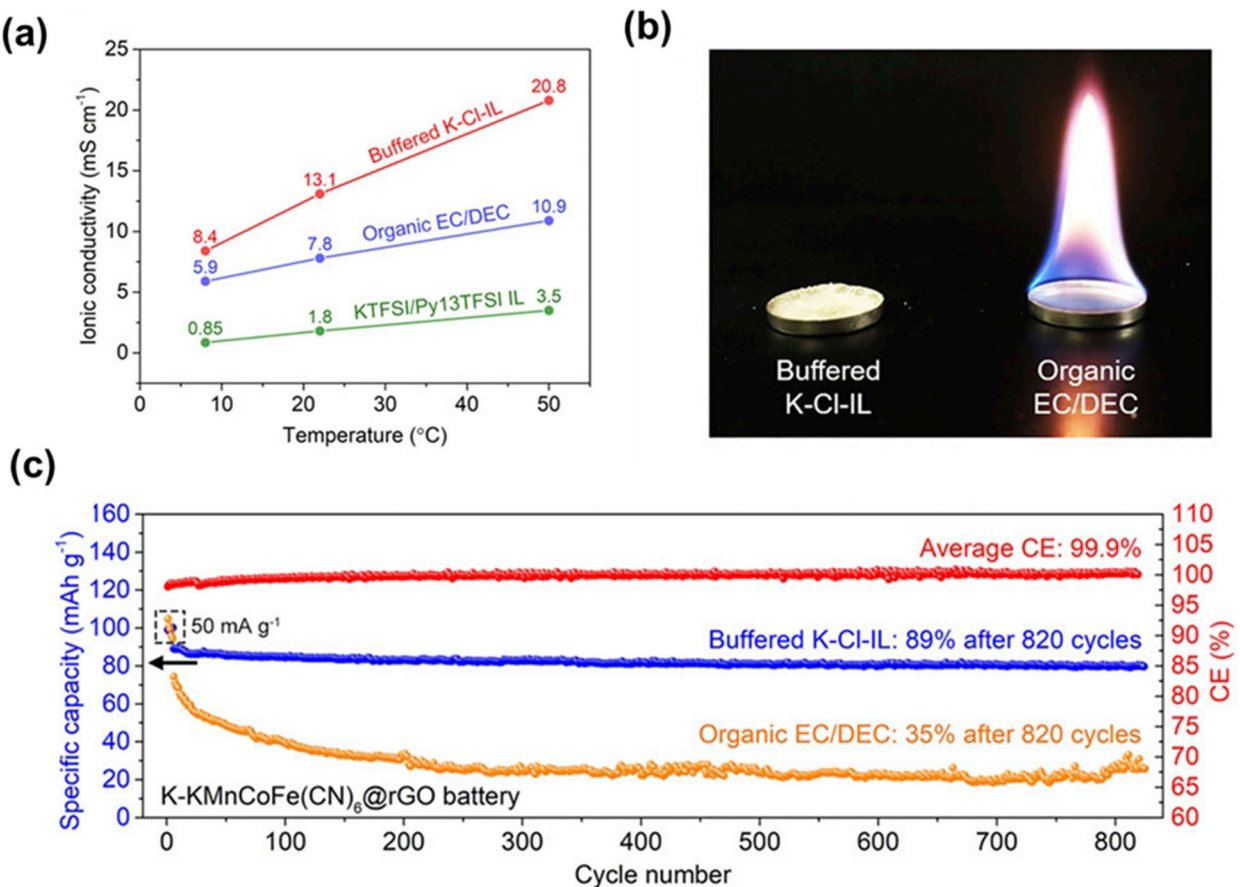


Figure 12. a) Ionic conductivities of buffered K-Cl-IL, 0.5 M KTFSI in Py13TFSI IL, and organic electrolyte, i.e., 0.9 M KPF6 in EC:DEC (1:1, v/v) at 8 °C, 22 °C, and 50 °C. b) Flammability test of buffered K-Cl-IL and conventional organic electrolytes. c) Cycling performance of potassium metal-KMnCoFe(CN)₆@rGO batteries using buffered K-Cl-IL and organic electrolytes at a specific current of 100 mA g⁻¹. Reproduced from Ref. [96] with permission. Copyright (2020) National Academy of Sciences.

ited high energy and power densities of 381 Wh kg⁻¹ and 1,350 W kg⁻¹, respectively, and an excellent cycling performance with 89% capacity retention after 820 cycles with an average CE of 99.9% (Figure 12c).^[96] The above-mentioned ILs demonstrated encouraging long cycle lives and electrochemical performance in PIBs when used with appropriate cathodes and anodes. Hence, ILs are a promising category of electrolytes for PIB application. However, intense research is required to develop this nascent technology for future practical applications.

6. Solid-State Electrolytes for PIBs

Traditional non-aqueous liquid electrolytes used in LIBs or PIBs exhibit excellent electrochemical properties with high ionic conductivities. However, the serious safety issues associated with the flammable and volatile organic liquid electrolytes in LIBs and PIBs have hindered their practical applications. Because of the high reactivity of potassium, PIBs pose a more serious safety issue than SIBs and LIBs. Solid-state electrolytes offer several advantages over organic liquid electrolytes such as better safety, high thermal stability, wider electrochemical

potential window, and longer cyclability.^[97,98] In particular, the ceramic based solid electrolyte has excellent mechanical properties and high ionic conductivity, while organic based solid electrolytes exhibit good flexibility and ease of processing.^[99,100] Therefore, solid-state electrolytes are considered promising alternatives to traditional non-aqueous electrolytes to overcome the safety issues in next-generation PIBs. However, the main challenges of LIBs and PIBs are their poor ionic conductivity and a poor interface between the electrodes and electrolyte. Solid polymer electrolytes (SPEs) and inorganic electrolytes, which are a type of solid-state electrolytes, have been studied for application in PIBs. Solid-state electrolytes significantly prevent the dissolution of organic active materials in non-aqueous electrolytes and enhance the cycle life of PIBs.^[101,102]

6.1. Solid Polymer Electrolytes (SPEs)

SPEs offer several unique advantages over traditional non-aqueous electrolytes such as, low cost, low weight, better processability, high flexibility, safety, high mechanical properties, and high thermal and chemical stability.^[103,104] However,

SPEs have been scarcely studied for application in PIBs, while extensive research has been conducted on SPEs for LIB application. The main drawback of SPEs is their poor ionic conductivity (10^{-5} – 10^{-7} S cm $^{-1}$) at RT.^[105,106] Most of the studies on SPEs have been carried out at high temperatures to achieve a high ionic conductivity. For instance, the minimum operating temperature of a PEO based SPE with a high ionic conductivity in LIBs was 60°C. However, the melting temperature of potassium (63.5°C) is lower than that of lithium and very close to the operating temperature of SPEs. This hinders the commercial application of SPE-based potassium metal batteries. Nevertheless, in this section, we mainly discuss the ionic conductivity and electrochemical properties of SPEs at moderate temperatures (60°C) for PIB application. Polymers such as PEO, polyacrylonitrile (PAN), polyvinyl alcohol (PVA), and polyvinylpyrrolidone (PVP) have been used as polymer hosts of SPEs for PIBs.

The first K-ion-conducting SPE, PEO-KAg₄I₅, was developed by Stevens.^[107] The SPE exhibited a high ionic conductivity of

$\sim 2 \times 10^{-3}$ S cm $^{-1}$ at RT. Besides, PEO was combined with a salt, KBrO₃, for application as an SPE.^[108] However, the SPE exhibited a low ionic conductivity of $\sim 7.74 \times 10^{-8}$ S cm $^{-1}$ at RT, which was insufficient for potassium ion conduction. Subsequently, Reddy et al. designed an SPE by mixing a blend of PVP and PVA with KBrO₃ by the solution cast method.^[109] The polyblend SPE with an optimised PVP:PVA:KBrO₃ ratio of 35:35:30 (w/w) exhibited a conductivity of 5×10^{-6} S cm $^{-1}$ at 33°C and a high K⁺ transport number of ~0.97. In addition, the authors investigated the effect of complexation of a PVC host with KBrO₃ salt as an SPE through the lone pair of electrons of chlorine atom in PVC on the solvation of the inorganic salt. The PVC+KBrO₃ polymer electrolyte (80:20, w/w) exhibited an ionic conductivity of $\approx 7 \times 10^{-8}$ S cm $^{-1}$ at 30°C.^[110] Furthermore, Fei et al. first reported a PPC-KFSI SPE with a nonwoven cellulose backbone (PPCB-SPEs) for application in PIBs.^[111] The optical image of PPCB-SPEs is shown in Figure 13a.^[111] The concentration of KFSI salt is the key factor affecting the ionic conductivity of SPEs. The experimental results showed that the ionic conductivity

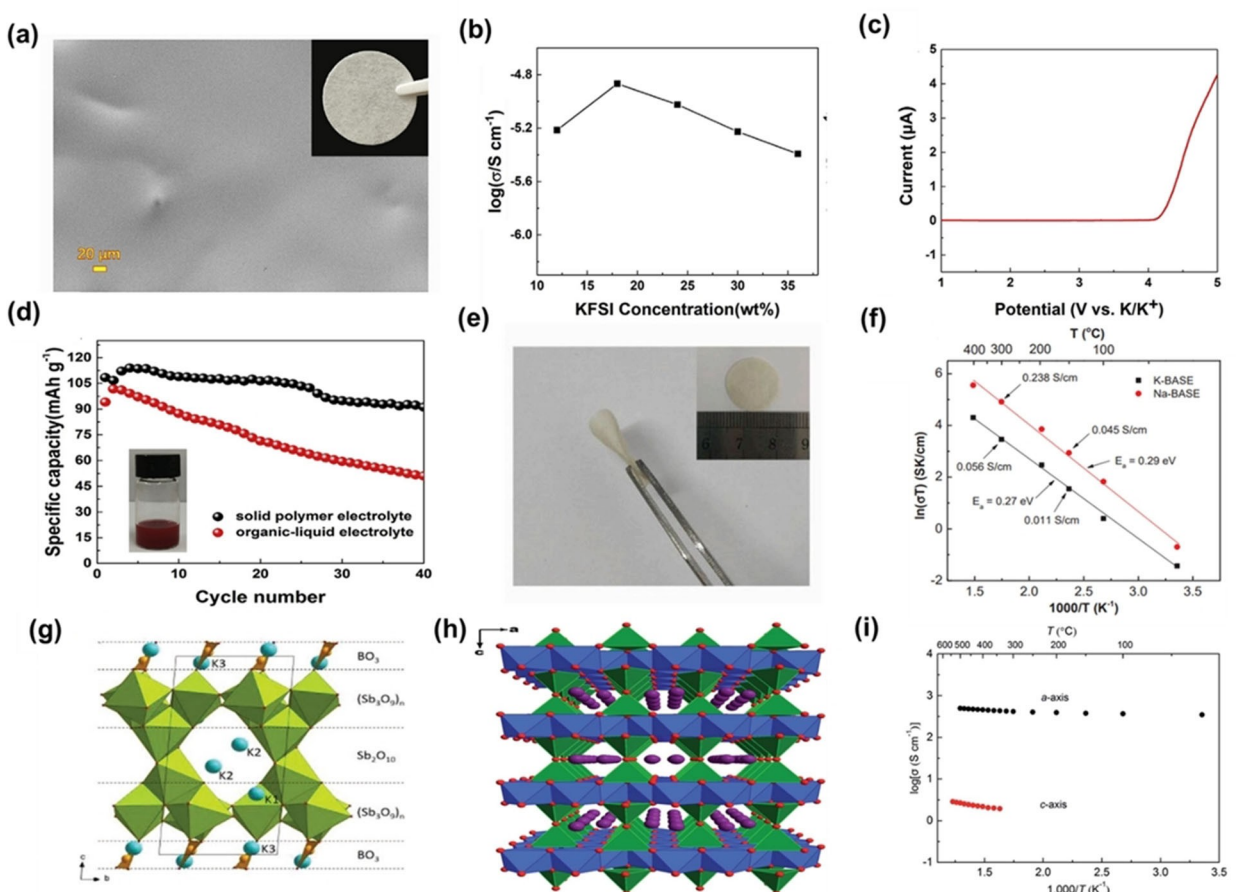


Figure 13. a) SEM image of PPCB-SPE. The inset is the digital image of PPCB-SPE. b) Ionic conductivity of a solid polymer with different concentrations of KFSI in PPC. c) LSV curve of a PPCB-SPE. d) Cycling performance of PTCDA with PPCB-SPE or organic liquid electrolyte at a current density of 20 mA g $^{-1}$. The inset is the digital image of the solubility test of PTCDA in 1 M KFSI in EC/DEC (1:1, v/v) electrolyte. Reproduced from Ref. [111] with permission. Copyright (2018) Elsevier. e) Flexibility of PEO-KFSI SPE. The inset shows the free-standing PEO-KFSI SPE. Reproduced from Ref. [112] with permission. Copyright (2019) Elsevier. f) Arrhenius plot of conductivities of K-BASE and Na-BASE samples. Reproduced from Ref. [113] with permission. Copyright (2015) Wiley-VCH. g) Structure of K₃Sb₂O₁₀(BO₃) and schematic representation of layer stacking. Reproduced from Ref. [114] with permission. Copyright (2018) Elsevier. h) 3D open framework structure of K₂Fe₄O₇ and intersecting 2D 6-ring channels filled with mobile potassium carriers viewed along the crystallographic b-axis. i) Arrhenius conductivity of potassium ions along the crystallographic a- and c-axes. Reproduced from Ref. [115] with permission. Copyright (2018) Royal Society of Chemistry.

first increased and then decreased with increasing salt concentration, and the SPEs exhibited a maximum ionic conductivity of $1.36 \times 10^{-5} \text{ Scm}^{-1}$ with an optimum salt concentration of 18 wt% at 20°C (Figure 13b).^[111] Furthermore, linear sweep voltammetry (LSV) measurements revealed the excellent electrochemical stability of PPCB-SPEs up to approximately 4.15 V vs. K/K⁺ (Figure 13c).^[111] The assembled all-solid-state potassium battery using a perylene-3,4,9,10-tetracarboxylic acid dianhydride (PTCDA) cathode and PPCB-SPE delivered a specific capacity of 113 mAhg⁻¹ after activation and maintained a capacity of 91.71 mAhg⁻¹ after 40 cycles with a slight capacity loss of ~0.4% per cycle. In contrast, the cell employing a non-aqueous electrolyte exhibited fast capacity decay at around 45.7%. The results confirmed that compared with organic electrolytes, SPEs improved capacity and cyclability of the cell by preventing the dissolution of the active material of the PTCDA cathode (Figure 13d).^[111] The same group later developed PEO-KFSI SPE membranes as solid-state electrolytes. The PEO-SPE membranes exhibited the highest ionic conductivity of $2.7 \times 10^{-4} \text{ Scm}^{-1}$ at 60°C at the optimum [EO]/[K⁺] molar ratio of ~10.^[112] The good flexibility of free standing PEO-KFSI SPE is shown in Figure 13e.^[112] The all-solid-state Ni₃S₂/Ni electrode with the PEO-KFSI electrolyte displayed outstanding cyclability with a high capacity of 307 mAhg⁻¹ after 100 cycles. The excellent cyclability was attributed to the PEO-based SPE, which could not only avoid the safety issues, but also suppressed the dissolution of polysulphides. Therefore, solid-state electrolytes can restrict the growth of metal dendrites and enhance the safety of batteries. However, because of the large size of potassium ions, the ionic conductivity of solid-state electrolytes is often low.

6.2. Inorganic Solid Electrolytes

The K⁺ ion conductivity of inorganic solid electrolytes is higher than that of SPEs. Therefore, various kinds of inorganic solid electrolytes have been developed over the past years. Lu et al. prepared a novel potassium-ion-conducting β-Al₂O₃ as a solid-state electrolyte (K-BASE) for K–S batteries.^[113] The K-BASE displayed high ionic conductivities of approximately 0.056 and 0.01 Scm^{-1} at 300 and 150°C, respectively (Figure 13f),^[113] and excellent wettability for potassium metal at 150°C compared with the wettability of Na-BASE for Na metal. Therefore, the resulting K–S batteries operated at a lower temperature of ~150°C and exhibited a better cycle life with negligible capacity decay over 1,000 cycles. The improved cycle life was attributed to the dense β-Al₂O₃ membrane that prevented interdiffusion and side reactions between the electrodes.

Generally, in materials with a suitable crystal structure consisting of one-dimensional (1D), two-dimensional (2D), and three-dimensional (3D) channels, alkali metal ions such as Li⁺, Na⁺, and K⁺ can move easily along the channels, resulting in a high ionic conductivity. K₃Sb₄O₁₀ (BO₃) (KSB) was fabricated in a single step by a solid-state reaction route.^[114] The K ion conductor with a 3D network structure and 1D tunnels along the *a*- and *b*-directions is shown in Figure 13g.^[114] KSB exhibited

a high K⁺ conductivity of $\sim 1.5 \times 10^{-4} \text{ Scm}^{-1}$ at 400°C due to a low activation energy of 0.325 eV. Furthermore, potassium ferrite (K₂Fe₄O₇) with a new 3D open framework was fabricated by a hydrothermal method.^[115] The crystal structure of K₂Fe₄O₇ had a 3D open framework with 2D 6-ring channels running parallel to the *a*- and *b*-axes and 1D 3-ring channels at the *c*-axis interconnected by hetero-polyhedra, as illustrated in Figure 13h.^[115] The electrolyte exhibited an excellent K⁺ ion conductivity of $5.0 \times 10^{-2} \text{ Scm}^{-1}$ at RT. Interestingly, the conductivity along the *a*-axis was as high as $3.5 \times 10^2 \text{ Scm}^{-1}$ for a single crystal at RT (Figure 13i).^[115] The difference in ionic conductivities along the *a*- and *c*-axes was mainly because the channels along the *a*-axis are sufficiently open and flat and have an optimum size compared with the channels along the *c*-axis. Therefore, the higher activation energy for migration of potassium ions at the *c*-axis resulted in a lower ionic conductivity in the *c*-direction. Furthermore, the K₂Fe₄O₇ electrode exhibited a stable potential up to 5 V, as determined by electrochemical characterisation. The all-solid-state PIB cell assembled with a potassium metal anode, Prussian blue cathode, and K₂Fe₄O₇ inorganic solid electrolyte exhibited a capacity retention of 78% over 50 cycles at a rate of 10 C, delivering a CE of approximately 100%. Further, Masese et al. proposed a high-potential cathode with a layered honeycomb structure synthesised by a solid-state reaction route.^[116] The K₂Mg₂TeO₆ potassium ion conductor with a layered tellurate structure displayed a high ionic conductivity of $\sim 38 \text{ mScm}^{-1}$ at 300°C. Xiao et al. explored a new potassium ion conductor, K₂CdO₂, for solid-state PIBs by computational techniques.^[117] The ionic conductivity of K₂CdO₂ was approximately $6.5 \times 10^{-15} \text{ Scm}^{-1}$ at 27°C. The Al doping of K₂CdO₂ led to the introduction of K⁺ vacancies, as K⁺ vacancy formation was the dominant step in the potassium ion diffusion process. The ionic conductivity of Al-doped K₂CdO₂ significantly improved to $2.2 \times 10^{-5} \text{ Scm}^{-1}$ at 27°C.

6.3. Hybrid/Composite Electrolytes

Gel polymer electrolytes (GPEs) are a type of composite electrolytes composed of polymer hosts and liquid electrolytes. PAN-based potassium iodide GPEs were fabricated by a solution casting method.^[118] FTIR spectroscopic analysis revealed a weak interaction between potassium ion and the C=O/C≡N functional group, while DSC analysis confirmed that the addition of KI and plasticisers increased the flexibility of GPEs by lowering the glass transition and melting temperatures of the polymer electrolytes. GPEs having an optimum mass ratio of 70:30 (PAN:KI) exhibited a high conductivity of $2.089 \times 10^{-5} \text{ Scm}^{-1}$ at 30°C. Subsequently, Gao et al. prepared a GPE with cross-linked poly(methyl methacrylate) (PMMA) and evaluated the electrochemical performance of PIBs using a polyaniline cathode and GPE (a liquid electrolyte was used for reference).^[119] The ionic conductivity of GPEs was $4.3 \times 10^{-3} \text{ Scm}^{-1}$ at RT (Figure 14b).^[119] LSV measurements showed that the upper limit of electrochemical stability window of GPE was 4.9 V vs. K/K⁺, which is enough to meet the requirements

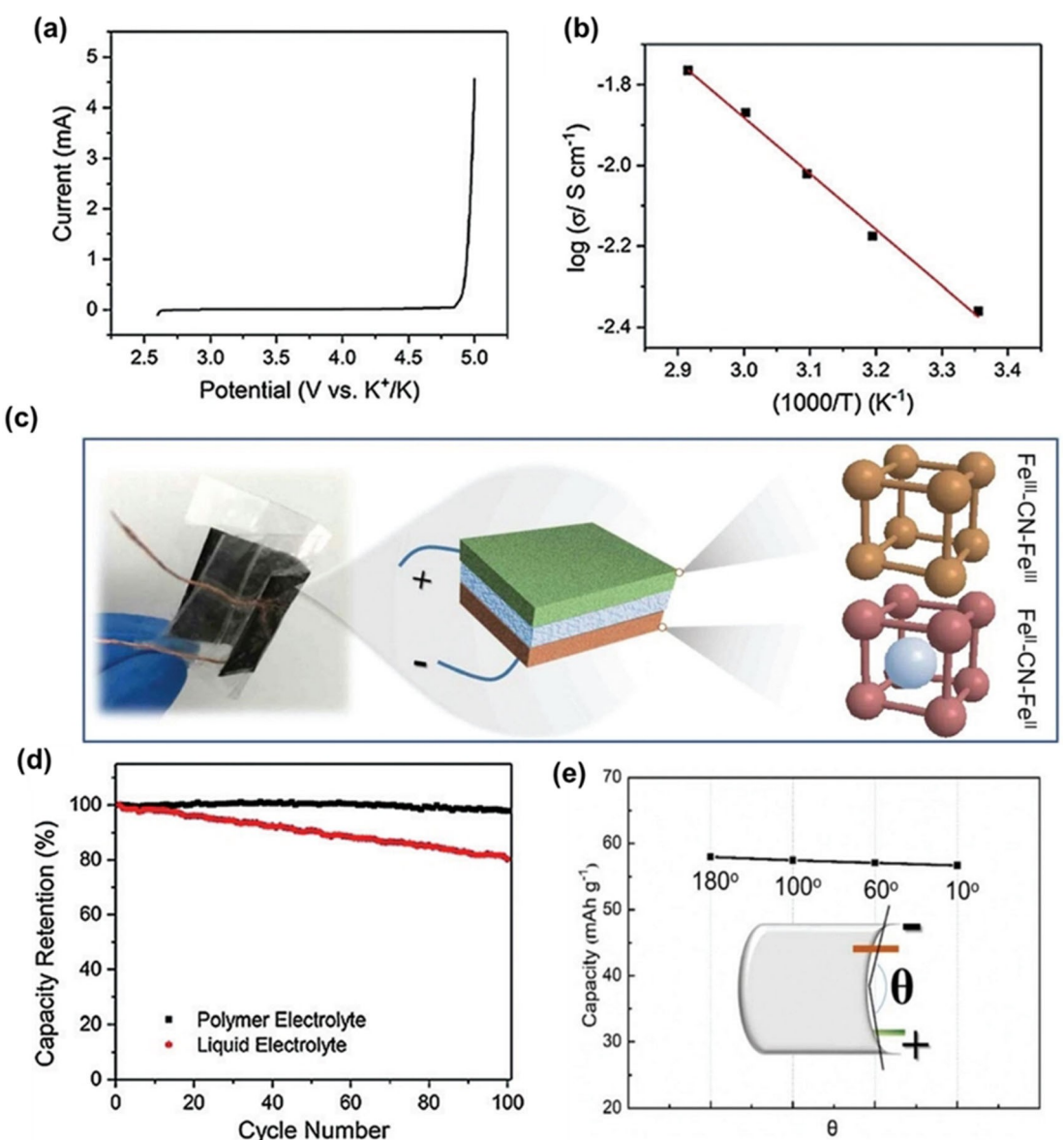


Figure 14. Electrochemical characterisation of a gel polymer electrolyte (GPE). a) LSV plot of GPE against a potassium metal anode at a scan rate of 1.0 mV s^{-1} . b) Ionic conductivity of GPE as a function of temperature. Reproduced from Ref. [119] with permission. Copyright (2018) Wiley-VCH. c) Photograph and schematic illustration of flexible solid-state symmetric K-ion cell with potassium Prussian blue (KPB) bipolar electrodes. Reproduced from Ref. [120] with permission. Copyright (2018) Royal Society of Chemistry. d) Cycling performance of polyaniline cathode at a current density of 50 mA g^{-1} . Reproduced from Ref. [119] with permission. Copyright (2018) Wiley-VCH. e) Discharge capacities of a full cell at different bending angles. Reproduced from Ref. [120] with permission. Copyright (2018) Royal Society of Chemistry.

of most cathode materials (Figure 14a).^[119] The polyaniline cathode cell exhibited a high-capacity retention of $\sim 98\%$ over 100 cycles at a specific current of 50 mA g^{-1} . In contrast, the organic liquid electrolyte-based cell exhibited 20% capacity fading (Figure 14d).^[119] The superior cycling stability of the polyaniline cell was attributed to GPE that significantly mitigated potassium dendrite growth and established a stable contact at the electrolyte/electrode interface. Besides, GPEs with appropriate flexibility and mechanical properties can help to realise flexible solid-state batteries. A flexible battery was fabricated using KPB@PPy@Cloth composite electrodes with PVA-KCl as the GPE, as shown in Figure 14c.^[120] The electrode displayed outstanding flexibility and insignificant capacity loss

under repeated folding conditions, as shown in Figure 14e.^[120] The flexible full cell exhibited excellent cyclability with a capacity retention of 82% after 200 cycles at a specific current of 500 mA g^{-1} .^[120] The research offered a new design for the advancement of flexible solid-state PIBs. However, for the realisation of all-solid-state PIBs, the interfacial compatibility, ionic conductivity, and electrochemical potential stability window need to be further improved. The ionic conductivities of various solid-state electrolytes are presented in Table 3. As can be seen, the potassium ion conductivity of inorganic solid electrolytes and composite electrolytes are higher than that of SPEs. However, for the commercial application of all-solid-state

Table 3. Ionic conductivities of various solid-state electrolytes.

| Classification | Electrolytes | Ionic conductivity [S cm^{-1}] | Ref. |
|------------------------------|---|---|-------|
| Solid polymer electrolytes | PVP + PVA + KBrO ₃ | 5×10^{-6} at 33 °C | [109] |
| | PVC + KBrO ₃ | 7×10^{-8} at 30 °C | [110] |
| | PEO-KBrO ₃ | 7.74×10^{-8} at RT | [108] |
| | PPC-KFSI | 1.36×10^{-5} at 20 °C | [111] |
| | PEO-KFSI | 1.14×10^{-5} at 40 °C | [112] |
| | PEO-KAg ₄ I ₅ | 2×10^{-3} at RT | [107] |
| Inorganic solid electrolytes | K ₂ Fe ₄ O ₇ | 5×10^{-2} (polycrystal) at 25 °C | [115] |
| | | 3.5×10^2 (single crystal) at 25 °C | [115] |
| | | 1.8 (single crystal) at 340 °C | [115] |
| | K ₂ Mg ₂ TeO ₆ | 3.8×10^{-2} at 300 °C | [116] |
| | K ₂ Sb ₂ O ₁₀ (BO ₃) | 1.5×10^{-4} at 400 °C | [114] |
| | Al-doped K ₂ CdO ₂ | 2.2×10^{-5} at 27 °C | [117] |
| Hybrid/composite electrolyte | K-BASE | 0.01 at 150 °C | [113] |
| | | 0.056 at 300 °C | [113] |
| | PMMA-KPF ₆ | 4.3×10^{-3} at RT | [119] |
| PIBs | PVA-KCl | 3.7×10^{-2} | [120] |
| | PAN-KI | 2.089×10^{-5} at 30 °C | [118] |

PIBs, future research should focus on the development of low-cost and sustainable solid-state electrolyte materials.

7. Full Cell Design

Full cells containing both anode and cathode perfectly are used to analyse the overall electrochemical properties of batteries. Because a full cell has the complete form of battery composed of anode, electrolyte (separator), and cathode, it enables the investigation of overall battery performance. In particular, before the commercialisation and practical utilisation of electrode materials, tests using full cell is essential. In our group, for the full cell study, we have used conventional CR2032-type two-electrodes coin cell and novel three-electrodes cell. From the literature, we found that commonly used cathode materials for full cell were Prussian blue, layered metal oxides, polyanionic compounds, and organic materials.^[39,127–130] Their counterpart anode materials were mainly carbonaceous materials, metallic alloy type materials, and others.^[6,131–137] It is worth noting that cathode and anode of the full cell often need a pre-potassiation process in the half-cell configuration using metallic potassium counter electrode before full cell assembling, to eliminate the adverse effects which are mainly observed in initial cycles. Furthermore, the N/P ratio needs to be optimised by controlling the mass loading of cathode and anode. Compared the half-cell fabrication, the full cell fabrication should be more careful, because reaction mechanisms on each electrode and pairing between anode and cathode need to be perfectly studied. In particular, the full cell performance is largely affected by the performance of cathode. Table 4 summarises different electrolytes used for full cell configuration and their performance reported in the literature.

8. Conclusion and Future Perspectives

Rechargeable LIBs are extensively used in a wide range of fields such as energy storage, portable electronics, and electric vehicles. However, due to the scarcity of Li resources, the cost of Li is steadily increasing, which may hinder the large-scale applications of LIBs in future. PIBs are a promising alternative to LIBs owing to their high energy density, abundance of potassium resources, and low cost. Nevertheless, PIB research is in nascent stages and several challenges especially regarding the electrolyte need to be overcome. Electrolytes directly affect the energy density, initial coulombic efficiency (CE), cycle life, safety, and operating conditions of batteries.

Electrolytes should have the same priority as the cathode, anode, and full cells in the design and development of PIBs. For commercialisation, the design of potential electrolytes should consider the following requirements: it should be i) highly ionic conductive, ii) electrochemically and thermally stable, iii) able to form sustainable and stable electrode/electrolyte interfaces, iv) cost-effective, and nontoxic.

Although aqueous PIBs are considerably safer and inexpensive, they exhibit a low energy density and fast dissolution of anodes and cathodes. Non-aqueous electrolytes exhibit a high potential range and high energy density, and are mainly classified as ester-based and ether-based electrolytes. Ester electrolytes give rise to severe side reactions due to the high reduction of potassium, resulting in poor cyclability and a low CE. In contrast, ether electrolytes improve stability, facilitate the formation of a stable SEI layer, and reduce side reactions. Unfortunately, ether electrolytes easily oxidise at high potentials, and thus reduce the cell potential and energy density of PIBs. To resolve this issue, KFSI-based electrolytes have been developed. KFSI-based electrolytes are beneficial for the formation of a stable, uniform, and robust SEI layer; however, its compatibility with the current collector needs to be further improved. Generally, highly concentrated electrolytes are beneficial for achieving a stable interface and inhibit corrosion reactions owing to the solvation effect. Furthermore, binary

Table 4. Summary of the electrolytes and cell performance of PIB full cells reported.

| Cathode-Anode | Electrolyte | Reversible discharge capacity [mAh g ⁻¹] | Cycle number | Capacity retention [mAh g ⁻¹] | Mass ratio | Ref. |
|--|---|--|--------------|---|------------|-------|
| P2-K _{0.75} [Mn _{0.8} Ni _{0.1} Fe _{0.1}]O ₂ -Hard Carbon | 0.5 M KPF ₆ in EC:DEC (1:1) | 60 | 1000 | ~37 | 1.2:1 | [128] |
| P2-K _{0.6} CoO ₂ -Graphite | 0.7 M KPF ₆ in EC:DEC (1:1) | 53 | 5 | ~50 | 2:1 | [130] |
| KMnHCF-Red P@C | 0.7 M KPF ₆ in EC:DEC (1:1) | 339 | 680 | 203 | 1.05:1.1 | [138] |
| KFe[Fe(CN) ₆]-SnP ₃ @C | 0.75 M KPF ₆ in EC:DEC (1:1) | 394 | 30 | 305 | 4:1 | [12] |
| KFe[Fe(CN) ₆]-OPDMC-1000 | 0.75 M KPF ₆ in EC:DEC (1:1) | 185.32 | 50 | 137.55 | 4:1 | [6] |
| P3-K _{0.5} [Mn _{0.85} Ni _{0.1} Co _{0.05}]O ₂ -graphite | 0.8 M KPF ₆ in EC:DEC (1:1) | 57 | 100 | 48 | 1:1.05 | [127] |
| K _{0.51} V ₂ O ₅ -Graphite | 0.8 M KPF ₆ in EC:DEC (1:1) | 80 | 100 | 67 | 1:1 | [139] |
| KFe[Fe(CN) ₆]-NCNF-650 ^[a] | 0.8 M KPF ₆ in EC:PC (1:1) | 197 | 30 | 190 | 4:1 | [131] |
| P2-K _{0.65} Fe _{0.5} Mn _{0.5} O ₂ -Hard Carbon | 0.9 M KPF ₆ in EC:DEC (1:1) | 76 | 100 | 61 | 2.1:1 | [143] |
| K _{1.81} Ni[Fe(CN) ₆] _{0.97} ·0.086H ₂ O-Graphite | 1 M KPF ₆ in EC:DEC:PC (1:1:1) | 43 | 100 | 37.8 | 1:2 | [141] |
| KFe[Fe(CN) ₆]-Graphite | 1 M KPF ₆ in Diglyme | ~49 | 2000 | ~30 | 1.6:1 | [144] |
| K _{1.69} Mn[Fe(CN) ₆] _{0.85} ·0.4H ₂ O-Hard carbon | 1.5 M KPF ₆ in Diglyme | 105 | 300 | 90 | – | [37] |
| KV ₅ O ₁₃ @rGO-V ₂ O ₅ -x@rGO | 2 M KFSI in EC:DEC (1:1) | 51 | 250 | 38.6 | 1:1 | [140] |
| K _{0.5} MnO ₂ -Graphite | 2.5 M KFSI in TEP | ~75 | 400 | 63 | 2:1 | [62] |
| PTCDA-Soft carbon ^[b] | 3 M KFSI in DME | ~75 | 3000 | 49 | – | [129] |
| PTCDA-Bi _{1.11} Sb _{0.89} S ₃ | 3 M KFSI in DME | 276 | 100 | 207 | – | [142] |
| PTCDA-Bi _{0.5} Sb _{0.5} @P | 4 M KFSI in DME | 280 | 100 | 154 | – | [135] |
| K ₄ Fe(CN) ₆ -BiSb@C | 5 M KFSI in DME | 396 | 200 | 361.6 | 7:1 | [136] |
| KFeHCF-Sb@C-3DP | 5 M KFSI in DME | 508 | 50 | 497 | 6:1 | [137] |
| K ₂ Mn[Fe(CN) ₆]-Graphite | 7 M KFSA in DME | 104 | 101 | 88 | 2.1:1 | [39] |

[a] NCNF: N-doped carbon nanofibers. [b] PTCDA: Perylene-3,4,9,10-tetracarboxylic dianhydride.

salt electrolytes significantly improve the cycle life and rate capability, stabilise the interface, and inhibit the corrosion of the current collector. Besides, they have a cost advantage over traditional concentrated electrolytes.

IL electrolytes exhibit negligible volatility, high electrochemical stability, and safety. In addition, they significantly improve the cycle life and rate capability, and are thus promising electrolytes for next-generation batteries. However, their application in PIBs has been scarcely studied. This is perhaps because of cost considerations as the IL electrolytes are relatively expensive. Therefore, the development of low-cost electrolytes for PIBs is a necessary future research direction. Besides, solid-state electrolytes exhibiting a wide electrochemical potential window and superior thermal stability are expected to enable reversible electrochemical discharge and charge reactions with high cell potentials. In particular, because of their high mechanical strength, solid-state electrolytes can reduce dendrite formation and improve interface stability. Hence, further improvement in their ionic conductivity and a facile fabrication process may render solid-state electrolytes competitive for application in PIBs. Herein, we have summarised each types of electrolyte for PIBs application with their different physical and electrochemical properties, as well as their future direction with a solution (Figure 15).

Several challenges remain in the development of suitable high-performance electrolytes for application in PIBs. The formation mechanism and charge transfer of the SEI layer in PIBs remain insufficiently understood and require intensive investigation. Advanced *in situ* analytical techniques, such as cryogenic electron microscopy and *in situ* transmission electron microscopy, and theoretical calculations are highly beneficial for analyse the charge transfer reaction at the

electrode/electrolyte interface, microstructure, and reaction mechanism. Second, the side reactions between potassium metal and the electrolyte need to be reduced. By enhancing the solubility of potassium salts in the ester electrolytes, a stable interface may be constructed and side reactions may be reduced. However, concentrated electrolytes can regulate polarisation and reduce side reactions by the solvation effect. KFSI electrolytes have been widely studied as they enable the formation of stable interfaces. Unfortunately, they corrode the current collector at high potentials. Furthermore, binary salt electrolytes are another promising option as they enable the formation of uniform, stable SEI layers and do not corrode the current collector. A new suitable potassium salt needs to be urgently developed. Finally, to ensure the safety of PIBs, flammable electrolytes need to be replaced with nonflammable electrolytes. ILs are viable medium-short-lived replacements for organic solvents in PIBs owing to their beneficial properties suitable for electrolytes, such as a high conductivity, electrochemical stability, wide temperature range, and low flammability and volatility. Among solid-state electrolytes, polymer-based electrolytes are highly likely to be employed in quasi-solid-state and all-solid-state batteries. However, their relatively low ionic conductivity and interfacial issues limit their applicability and appeal to researchers. To increase the ionic conductivity, special additives or other novel polymer hosts can be used in SPEs. Further research in the chemistry of electrolytes and electrode/electrolyte interfaces is expected to help in the realisation of low-cost, high-energy density PIBs, taking them a step closer to commercialisation.

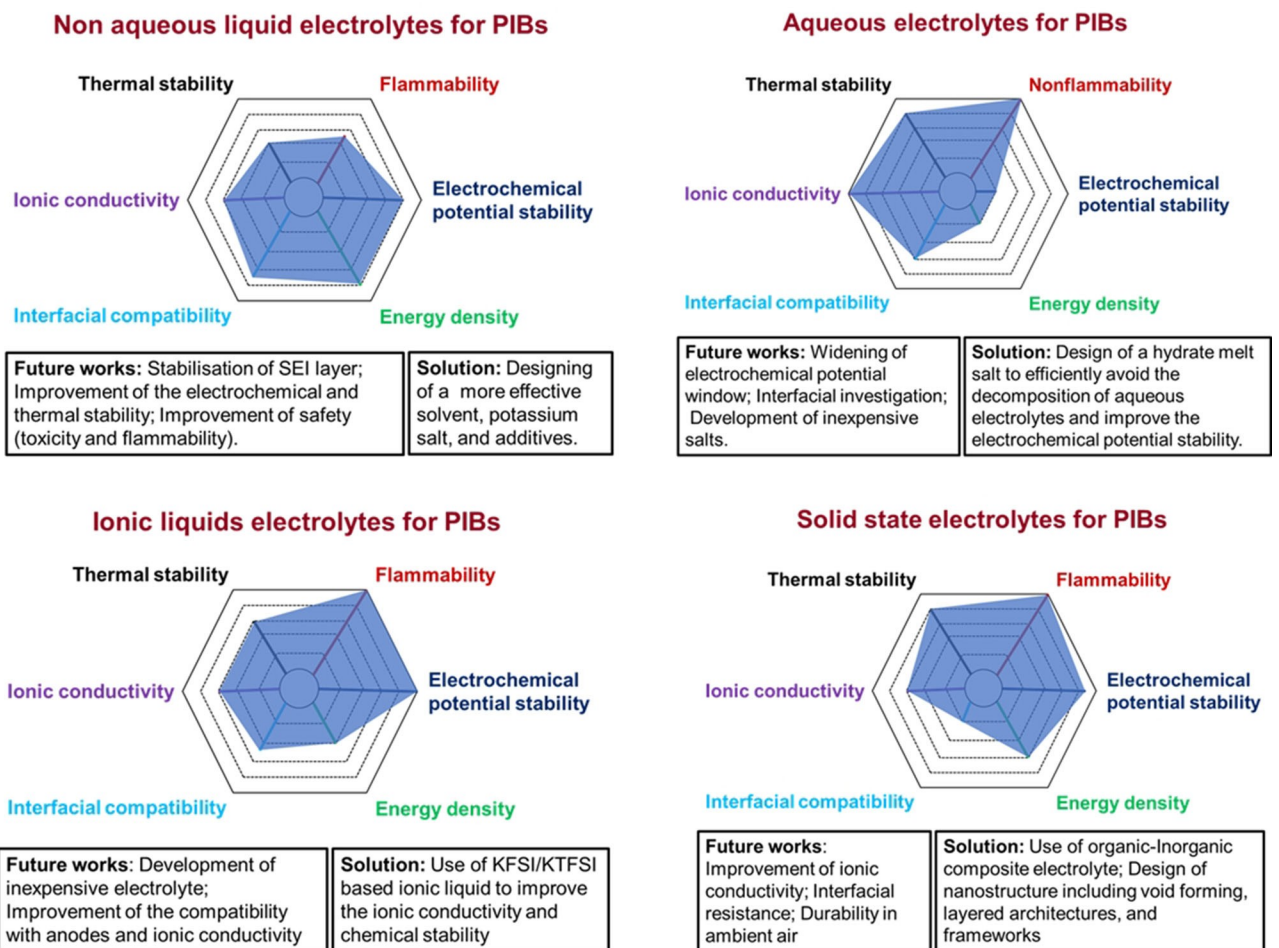


Figure 15. Comparison of electrolytes for PIBs in aspects of their different physical, electrochemical properties, and future direction with a solution.

Acknowledgements

This research was supported by the National Research Foundation of Korea (NRF) (grant nos. 2019R1A2C1084020 and 2018R1A5A1025224).

Conflict of Interest

The authors declare no conflict of interest.

Keywords: potassium-ion batteries • electrolytes • design strategies • stability • additive

- [1] Y. Tang, Y. Zhang, W. Li, B. Ma, X. Chen, *Chem. Soc. Rev.* **2015**, *44*, 5926.
- [2] G. Harper, R. Sommerville, E. Kendrick, L. Driscoll, P. Slater, R. Stolkin, A. Walton, P. Christensen, O. Heidrich, S. Lambert, A. Abbott, K. Ryder, L. Gaines, P. Anderson, *Nature* **2019**, *575*, 75.
- [3] R. Verma, C. J. Park, R. Kothandaraman, U. V. Varadaraju, *Electrochim. Acta* **2017**, *258*, 1445–1452.
- [4] R. Verma, R. Kothandaraman, U. V. Varadaraju, *Appl. Surf. Sci.* **2017**, *418*, 30–39.

- [5] T. Hosaka, K. Kubota, A. S. Hameed, S. Komaba, *Chem. Rev.* **2020**, *120*, 6358–6466.
- [6] R. Verma, Y. N. Singhbabu, P. N. Didwal, A. Nguyen, J. Kim, C. Park, *Batteries & Supercaps* **2020**, *3*, 1099–1111.
- [7] C. Vaalma, D. Buchholz, M. Weil, S. Passerini, *Nat. Rev. Mater.* **2018**, *3*, 18013.
- [8] P. N. Didwal, R. Verma, C. W. Min, C. J. Park, *J. Power Sources* **2019**, *413*, 1–10.
- [9] R. Verma, R. K. Raman, U. V. Varadaraju, *J. Solid State Electrochem.* **2016**, *20*, 1501–1505.
- [10] X. M. Pham, D. T. Ngo, H. T. T. Le, P. N. Didwal, R. Verma, C. W. Min, C. N. Park, C. J. Park, *Nanoscale* **2018**, *10*, 19399–19408.
- [11] S. Sinha, P. N. Didwal, D. K. Nandi, R. Verma, J. Y. Cho, S. H. Kim, C. J. Park, J. Heo, *Small* **2019**, *15*, 1900595.
- [12] R. Verma, P. N. Didwal, H. S. Ki, G. Cao, C. J. Park, *ACS Appl. Mater. Interfaces* **2019**, *11*, 26976–26984.
- [13] S. Tan, F. Xiong, J. Wang, Q. An, L. Mai, *Mater. Horiz.* **2020**, *7*, 1971–1995.
- [14] C. Kuang, W. Zeng, Y. Li, *Nanosci. Nanotechnol.* **2019**, *19*, 12–25.
- [15] X. Zou, P. Xiong, J. Zhao, J. Hu, Z. Liu, Y. Xu, *Phys. Chem. Chem. Phys.* **2017**, *19*, 26495–26506.
- [16] A. Eftekhari, Z. Jian, X. Ji, *ACS Appl. Mater. Interfaces* **2017**, *9*, 4404–4419.
- [17] Y. Marcus, *Pure Appl. Chem.* **1985**, *57*, 1129–1132.
- [18] Y. Matsuda, H. Nakashima, M. Morita, Y. Takasu, *J. Electrochem. Soc.* **1981**, *128*, 2552–2556.
- [19] R. L. Rudnick, S. Gao, *Composition of the Continental Crust*, Elsevier, 2003, 3, treatise on geochemistry (ISBN: 0-08-044338-9); pp. 1–64.
- [20] M. Okoshi, Y. Yamada, S. Komaba, A. Yamada, H. Nakai, *J. Electrochem. Soc.* **2017**, *164*, A54–A60.
- [21] Z. Jian, W. Luo, X. Ji, *J. Am. Chem. Soc.* **2015**, *137*, 11566–11569.

- [22] J. Y. Hwang, S. T. Myung, Y. K. Sun, *Adv. Funct. Mater.* **2018**, *28*, 1802938.
- [23] W. Zhang, Y. Liu, Z. Guo, *Sci. Adv.* **2019**, *5*, eaav7412.
- [24] Y. Hamon, T. Brousse, F. Jousse, P. Topart, P. Buvat, D. M. Schleich, *J. Power Sources* **2001**, *97–98*, 185–187.
- [25] J. Zhang, T. Liu, X. Cheng, M. Xia, R. Zheng, N. Peng, H. Yu, M. Shui, J. Shu, *Nano Energy* **2019**, *60*, 340–361.
- [26] J. Zhang, X. Yao, R. K. Misra, Q. Cai, Y. Zhao, *J. Mater. Sci. Technol.* **2020**, *44*, 237–257.
- [27] C. Zhong, Y. Deng, W. Hu, J. Qiao, L. Zhang, J. Zhang, *Chem. Soc. Rev.* **2015**, *44*, 7484–7539.
- [28] J. B. Goodenough, P. Singh, *J. Electrochem. Soc.* **2015**, *162*, A2387–A2392.
- [29] D. W. Shin, M. D. Guiver, Y. M. Lee, *Chem. Rev.* **2017**, *117*, 4759–4805.
- [30] L. Deng, Y. Zhang, R. Wang, M. Feng, X. Niu, L. Tan, Y. Zhu, *ACS Appl. Mater. Interfaces* **2019**, *11*, 22449–22456.
- [31] H. S. Kim, R. Verma, J. Kim, C. J. Park, *ACS Sustainable Chem. Eng.* **2020**, *8*, 11123–11132.
- [32] K. Yoshida, M. Nakamura, Y. Kazue, N. Tachikawa, S. Tsuzuki, S. Seki, K. Dokko, M. Watanabe, *J. Am. Chem. Soc.* **2011**, *133*, 13121–13129.
- [33] L. Suo, O. Borodin, T. Gao, M. Olguin, J. Ho, X. Fan, C. Luo, C. Wang, K. Xu, *Science* **2015**, *350*, 938.
- [34] N. S. Katorova, S. S. Fedotov, D. P. Rupasov, N. D. Luchinin, B. Delattre, Y. M. Chiang, A. M. Abakumov, K. J. Stevenson, *ACS Appl. Mater. Interfaces* **2019**, *2*, 6051–6059.
- [35] S. Liu, J. Mao, L. Zhang, W. K. Pang, A. Du, Z. Guo, *Adv. Mater.* **2020**, *33*, 2006313.
- [36] T. Hosaka, K. Kubota, H. Kojima, S. Komaba, *Chem. Commun.* **2018**, *54*, 8387–8390.
- [37] X. Wu, Y. Chen, Z. Xing, C. W. K. Lam, S. S. Pang, W. Zhang, Z. Ju, *Adv. Energy Mater.* **2019**, *9*, 1900343.
- [38] E. Zhang, X. Jia, B. Wang, J. Wang, X. Yu, B. Lu, *Adv. Sci.* **2020**, *7*, 2000470.
- [39] W. Zhang, Y. Yan, Z. Xie, Y. Yang, Y. Xiao, M. Zheng, H. Hu, H. Dong, Y. Liu, Y. Liang, *J. Colloid Interface Sci.* **2020**, *561*, 195–202.
- [40] W. Zhang, W. K. Pang, V. Sencadas, Z. Guo, *Joule* **2018**, *2*, 1534.
- [41] W. Zhang, Z. Wu, J. Zhang, G. Liu, N. H. Yang, R. S. Liu, W. K. Pang, W. Li, Z. Guo, *Nano Energy* **2018**, *53*, 967–974.
- [42] J. Xie, J. Li, W. Zhuo, W. Mai, *Mater. Today* **2020**, *6*, 100035.
- [43] L. Fan, R. Ma, Q. Zhang, X. Jia, B. Lu, *Angew. Chem. Int. Ed.* **2019**, *58*, 10500–10505; *Angew. Chem.* **2019**, *131*, 10610–10615.
- [44] K. Xu, *Chem. Rev.* **2014**, *114*, 11503–11618.
- [45] X. Liu, G. A. Elia, X. Gao, B. Qin, H. Zhang, S. Passerini, *Batteries & Supercaps* **2020**, *3*, 261–267.
- [46] T. Hosaka, T. Matsuyama, K. Kubota, S. Yasuno, S. Komaba, *ACS Appl. Mater. Interfaces* **2020**, *12*, 34873–34881.
- [47] Q. Zhang, J. Mao, W. K. Pang, T. Zheng, V. Sencadas, Y. Chen, Y. Liu, Z. Guo, *Adv. Energy Mater.* **2018**, *8*, 1703288.
- [48] N. Xiao, W. D. McCulloch, Y. Wu, *J. Am. Chem. Soc.* **2017**, *139*, 9475–9478.
- [49] H. Wang, D. Yu, X. Wang, Z. Niu, M. Chen, L. Cheng, W. Zhou, L. Guo, *Angew. Chem. Int. Ed.* **2019**, *58*, 16451–16455; *Angew. Chem.* **2019**, *131*, 16603–16607.
- [50] M. Li, C. Wang, Z. Chen, K. Xu, J. Lu, *Chem. Rev.* **2020**, *120*, 6783–6819.
- [51] B. Ji, F. Zhang, X. Song, Y. Tang, *Adv. Mater.* **2017**, *29*, 1700519.
- [52] T. A. Pham, K. E. Kweon, A. Samanta, V. Lordi, J. E. Pask, *J. Phys. Chem. C* **2017**, *121*, 21913–21920.
- [53] J. Zhao, X. Zou, Y. Zhu, Y. Xu, C. Wang, *Adv. Funct. Mater.* **2016**, *26*, 8103–8110.
- [54] Y. Lei, L. Qin, R. Liu, K. C. Lau, Y. Wu, D. Zhai, B. Li, F. Kang, *ACS Appl. Mater. Interfaces* **2018**, *1*, 1828–1833.
- [55] A. Ponrouche, E. Marchante, M. Courty, J. M. Tarascon, M. R. Palacín, *Energy Environ. Sci.* **2012**, *5*, 8572–8583.
- [56] A. Ponrouche, R. Dédryvère, D. Monti, A. E. Demet, J. M. Ateba Mba, L. Croguennec, C. Masquelier, P. Johansson, M. R. Palacín, *Energy Environ. Sci.* **2013**, *6*, 2361–2369.
- [57] D. M. Seo, S. Reininger, M. Kutcher, K. Redmond, W. B. Euler, B. L. Lucht, *J. Phys. Chem. C* **2015**, *119*, 14038–14046.
- [58] S. Liu, J. Mao, Q. Zhang, Z. Wang, W. K. Pang, L. Zhang, A. Du, V. Sencadas, W. Zhang, Z. Guo, *Angew. Chem. Int. Ed.* **2020**, *59*, 3638–3644; *Angew. Chem.* **2020**, *132*, 3667–3673.
- [59] L. Deng, L. Deng, T. Wang, Y. Hong, M. Feng, R. Wang, J. Zhang, Q. Zhang, J. Wang, L. Zeng, Y. Zhu, Y. Zhu, L. Guo, *ACS Energy Lett.* **2020**, *5*, 1916–1922.
- [60] Y. Yamada, A. Yamada, *J. Electrochem. Soc.* **2015**, *162*, A2406–A2423.
- [61] J. Wu, Q. Zhang, S. Liu, J. Long, Z. Wu, W. Zhang, W. K. Pang, V. Sencadas, R. Song, W. Song, J. Mao, Z. Guo, *Nano Energy* **2020**, *77*, 105118.
- [62] R. Zhang, J. Bao, Y. Wang, C. F. Sun, *Chem. Sci.* **2018**, *9*, 6193–6198.
- [63] J. Xie, Y. Zhu, N. Zhuang, X. Li, X. Yuan, J. Li, G. Hong, W. Mai, *J. Mater. Chem. A* **2019**, *7*, 19332–19341.
- [64] L. Wang, J. Yang, J. Li, T. Chen, S. Chen, Z. Wu, J. Qiu, B. Wang, P. Gao, X. Niu, H. Li, *J. Power Sources* **2019**, *409*, 24–30.
- [65] Z. Wang, K. Dong, D. Wang, S. Luo, Y. Liu, Q. Wang, Y. Zhang, A. Hao, C. Shi, N. Zhao, *J. Mater. Chem. A* **2019**, *7*, 14309–14318.
- [66] B. Li, J. Zhao, Z. Zhang, C. Zhao, P. Sun, P. Bai, J. Yang, Z. Zhou, Y. Xu, *Adv. Funct. Mater.* **2019**, *29*, 1807137.
- [67] L. Wang, J. Zou, S. Chen, G. Zhou, J. Bai, P. Gao, Y. Wang, X. Yu, J. Li, Y. S. Hu, H. Li, *Energy Storage Mater.* **2018**, *12*, 216–222.
- [68] C. Xu, G. Hernández, S. Abbrecht, L. Kobera, R. Konefal, J. Brus, K. Edström, D. Brandell, J. Mindemark, *ACS Appl. Mater. Interfaces* **2019**, *2*, 4925–4935.
- [69] J. Qian, Y. Chen, L. Wu, Y. Cao, X. Ai, H. Yang, *Chem. Commun.* **2012**, *48*, 7070–7072.
- [70] G. He, L. F. Nazar, *ACS Energy Lett.* **2017**, *2*, 1122–1127.
- [71] X. Bie, K. Kubota, T. Hosaka, K. Chihara, S. Komaba, *J. Mater. Chem. A* **2017**, *5*, 4325–4330.
- [72] H. Kim, J. C. Kim, M. Bianchini, D. H. Seo, J. Rodriguez-Garcia, G. Ceder, *Adv. Energy Mater.* **2018**, *8*, 1702384.
- [73] P. Peljo, H.-H. Girault, *Energy Environ. Sci.* **2018**, *11*, 2306–2309.
- [74] L. Liu, Z. Lin, J. Y. Chane-Ching, H. Shao, P. L. Taberna, P. Simon, *Energy Storage Mater.* **2019**, *19*, 306–313.
- [75] H. Che, S. Chen, Y. Xie, H. Wang, K. Amine, X. Z. Liao, Z. F. Ma, *Energy Environ. Sci.* **2017**, *10*, 1075–1101.
- [76] M.-T. F. Rodrigues, G. Babu, H. Gullapalli, K. Kalaga, F. N. Sayed, K. Kato, J. Joyner, P. M. Ajayan, *Nat. Energy* **2017**, *2*, 1.
- [77] R. A. Adams, A. Varma, V. G. Pol, *J. Power Sources* **2019**, *410–411*, 124–131.
- [78] H. Kim, J. Hong, K. Y. Park, H. Kim, S. W. Kim, K. Kang, *Chem. Rev.* **2014**, *114*, 11788–11827.
- [79] Y. Liang, Y. Jing, S. Gheytani, K. Y. Lee, P. Liu, A. Facchetti, Y. Yao, *Nat. Mater.* **2017**, *16*, 841.
- [80] H. Chen, Z. Zhang, Z. Wei, G. Chen, X. Yang, C. Wang, F. Du, *Sustain. Energy Fuels* **2020**, *4*, 128–131.
- [81] L. Jiang, Y. Lu, C. Zhao, L. Liu, J. Zhang, Q. Zhang, X. Shen, J. Zhao, X. Yu, H. Li, X. Huang, L. Chen, Y. S. Hu, *Nat. Energy* **2019**, *4*, 495.
- [82] M. Wang, H. Wang, H. Zhang, X. Li, *J. Energy Chem.* **2020**, *48*, 14–20.
- [83] J. Li, H. Zhao, J. Wang, N. Li, M. Wu, Q. Zhang, Y. Du, *Nano Energy* **2019**, *62*, 876–882.
- [84] Z. Jian, Y. Liang, I. A. R. Pérez, Y. Yao, X. Ji, *Electrochem. Commun.* **2016**, *71*, 5–8.
- [85] D. P. Leonard, Z. Wei, G. Chen, F. Du, X. Ji, *ACS Energy Lett.* **2018**, *3*, 373–374.
- [86] K. Yoshii, T. Masese, M. Kato, K. Kubota, H. Senoh, M. Shikano, *ChemElectroChem* **2019**, *6*, 3901–3910.
- [87] T. Masese, K. Yoshii, Y. Yamaguchi, T. Okumura, Z. D. Huang, M. Kato, K. Kubota, J. Furutani, Y. Oriksa, H. Senoh, H. Sakaebe, M. Shikano, *Nat. Commun.* **2018**, *9*, 1.
- [88] T. Yamamoto, K. Matsumoto, R. Hagiwara, T. Nohira, *J. Phys. Chem. C* **2017**, *121*, 18450–18458.
- [89] H. Onuma, K. Kubota, S. Muratsubaki, T. Hosaka, R. Tatara, T. Yamamoto, K. Matsumoto, T. Nohira, R. Hagiwara, H. Oji, S. Yasuno, S. Komaba, *ACS Energy Lett.* **2020**, *5*, 2849–2857.
- [90] M. Arnaiz, A. Bothe, S. Dsoke, A. Balducci, J. Ajuria, *J. Electrochem. Soc.* **2019**, *166*, A3504–A3510.
- [91] R. M. De Souza, L. J. A. De Siqueira, M. Karttunen, L. G. Dias, *J. Chem. Inf. Model.* **2020**, *60*, 485–499.
- [92] T. Yamamoto, T. Nohira, *Chem. Commun.* **2020**, *56*, 2538–2541.
- [93] H. Sun, P. Liang, G. Zhu, W. H. Hung, Y. Y. Li, H. C. Tai, C. L. Huang, J. Li, Y. Meng, M. Angell, C. A. Wang, H. Dai, *Proc. Natl. Acad. Sci. USA* **2020**, *117*, 27847.
- [94] H. T. T. Le, D. T. Ngo, P. N. Didwal, J. G. Fisher, C. N. Park, I. D. Kim, C. J. Park, *J. Mater. Chem. A* **2019**, *7*, 3150–3160.
- [95] F. Lv, Z. Wang, L. Shi, J. Zhu, K. Edström, J. Mindemark, S. Yuan, *J. Power Sources* **2019**, *441*, 227175.
- [96] H. T. T. Le, D. T. Ngo, R. S. Kalubarme, G. Cao, C. N. Park, C. J. Park, *ACS Appl. Mater. Interfaces* **2016**, *8*, 20710–20719.
- [97] B. Zhang, M. Weng, Z. Lin, Y. Feng, L. Yang, L. W. Wang, F. Pan, *Small* **2020**, *16*, 1906374.
- [98] C. Jiang, H. Li, C. Wang, *Sci. Bull.* **2017**, *62*, 1473–1490.

- [99] R. Rajagopalan, Y. Tang, X. Ji, C. Jia, H. Wang, *Adv. Funct. Mater.* **2020**, *30*, 1909486.
- [100] J. H. Cha, P. N. Didwal, J. M. Kim, D. R. Chang, C. J. Park, *J. Membr. Sci.* **2020**, *595*, 117538.
- [101] H. Wang, L. Sheng, G. Yasin, L. Wang, H. Xu, X. He, *Energy Storage Mater.* **2020**, *33*, 188–215.
- [102] P. N. Didwal, Y. N. Singhbabu, R. Verma, B. Sung, G. Lee, J. Lee, D. Rye, C. Park, *Energy Storage Mater.* **2021**, *37*, 476.
- [103] W. Liu, S. W. Lee, D. Lin, F. Shi, S. Wang, A. D. Sendek, Y. Cui, *Nat. Energy* **2017**, *2*, 17035.
- [104] J. R. Stevens, B. E. Mellander, *Solid State Ionics* **1986**, *21*, 203–206.
- [105] T. Sreekanth, M. Jaipal Reddy, U. V. Subba Rao, *J. Power Sources* **2001**, *93*, 268–272.
- [106] C. V. S. Reddy, A. K. Sharma, V. V. R. N. Rao, *Ionics* **2004**, *10*, 142.
- [107] T. Janaki Rami Reddy, V. B. S. Achari, A. K. Sharma, V. V. R. Narasimha Rao, *Ionics* **2007**, *13*, 435–439.
- [108] H. Fei, Y. Liu, Y. An, X. Xu, G. Zeng, Y. Tian, L. Ci, B. Xi, S. Xiong, J. Feng, *J. Power Sources* **2018**, *399*, 294–298.
- [109] H. Fei, Y. Liu, Y. An, X. Xu, J. Zhang, B. Xi, S. Xiong, J. Feng, *J. Power Sources* **2019**, *433*, 226697.
- [110] X. Lu, M. E. Bowden, V. L. Sprenkle, J. Liu, *Adv. Mater.* **2015**, *27*, 5915–5922.
- [111] J. M. Doux, L. Leguay, A. Le Gal La Salle, O. Joubert, E. Quarez, *Solid State Ionics* **2018**, *324*, 260–266.
- [112] H. Yuan, H. Li, T. Zhang, G. Li, T. He, F. Du, S. Feng, *J. Mater. Chem. A* **2018**, *6*, 8413–8418.
- [113] T. Masese, K. Yoshii, Y. Yamaguchi, T. Okumura, Z.-D. Huang, M. Kato, K. Kubota, J. Furutani, Y. Orikasa, H. Senoh, H. Sakaebi, M. Shikano, *Nat. Commun.* **2018**, *9*, 3823.
- [114] R. Xiao, H. Li, L. Chen, *J. Mater. Chem. A* **2020**, *8*, 5157–5162.
- [115] N. Krishna Jyothi, K. K. Venkataratnam, P. Narayana Murty, K. Vijaya Kumar, *Bull. Mater. Sci.* **2016**, *39*, 1047.
- [116] H. Gao, L. Xue, S. Xin, J. B. Goodenough, *Angew. Chem. Int. Ed.* **2018**, *130*, 5447–5451.
- [117] K. Lu, H. Zhang, S. Gao, Y. Cheng, H. Ma, *Nanoscale* **2018**, *10*, 20754–20760.
- [118] L. Fan, S. Chen, R. Ma, J. Wang, L. Wang, Q. Zhang, E. Zhang, Z. Liu, B. Lu, *Small* **2018**, *14*, 1801806.
- [119] K. Han, Z. Liu, P. Li, Q. Yu, W. Alex Wang, C. Y. Lao, D. He, W. Zhao, G. Suo, H. Guo, L. Song, M. Qin, X. Qu, *Energy Storage Mater.* **2019**, *22*, 185–193.
- [120] Y. Qian, S. Jiang, Y. Li, Z. Yi, J. Zhou, J. Tian, N. Lin, Y. Qian, *Energy Storage Mater.* **2020**, *29*, 341–349.
- [121] F. Liu, J. Meng, F. Xia, Z. Liu, H. Peng, C. Sun, L. Xu, G. Van Tendeloo, L. Mai, J. Wu, *J. Mater. Chem. A* **2020**, *8*, 18079–18086.
- [122] Q. Liu, F. Han, J. Zhou, Y. Li, L. Chen, F. Zhang, D. Zhou, C. Ye, J. Yang, X. Wu, J. Liu, *ACS Appl. Mater. Interfaces* **2020**, *12*, 20838–20848.
- [123] H. Zhang, C. Luo, H. He, H.-H. Wu, Li. Zhang, Q. Zhang, H. Wang, M-S. Wang, *Nanoscale Horiz.* **2020**, *5*, 895–903.
- [124] J. Hao, K. Xiong, J. Zhou, A. M. Rao, X. Wang, H. Liu, B. Lu, *Energy Environ. Mater.* **2020**, *0*, 1–9.
- [125] J. Y. Hwang, J. Kim, T. Y. Yu, H. G. Jung, J. Kim, K. H. Kim, Y. K. Sun, *J. Mater. Chem. A* **2019**, *7*, 21362–21370.
- [126] L. Fan, R. Ma, J. Wang, H. Yang, B. Lu, *Adv. Mater.* **2018**, *30*, 1805486.
- [127] H. Kim, J. C. Kim, S. H. Bo, T. Shi, D. H. Kwon, G. Ceder, *Adv. Energy Mater.* **2017**, *7*, 1700098.
- [128] Y. Xu, C. Zhang, M. Zhou, Q. Fu, C. Zhao, M. Wu, Y. Lei, *Nat. Commun.* **2018**, *9*, 1720.
- [129] H. Ding, J. Zhou, A. M. Rao, B. Lu, *Natl. Sci. Rev.* **2020**, DOI: 10.1093/nsr/nwaa276.
- [130] Q. Zhang, X. Cheng, C. Wang, A. M. Rao, B. Lu, *Energy Environ. Sci.* **2021**, *14*, 965–974.
- [131] T. Wang, D. Shen, H. Liu, H. Chen, Q. Liu, B. Lu, *ACS Appl. Mater. Interfaces* **2020**, *12*, 57907.
- [132] K. T. Chen, H. Y. Tuan, *ACS Nano* **2020**, *14*, 11648–11661.
- [133] P. Xiong, J. Wu, M. Zhou, Y. Xu, *ACS Nano* **2020**, *14*, 1018–1026.
- [134] X. D. He, Z. H. Liu, J. Y. Liao, X. Ding, Q. Hu, L. N. Xiao, S. Wang, C. H. Chen, *J. Mater. Chem. A* **2019**, *7*, 9629–9637.
- [135] W. C. Chang, J. H. Wu, K. T. Chen, H. Y. Tuan, *Adv. Sci.* **2019**, *6*, 1801354.
- [136] Y. H. Zhu, Q. Zhang, X. Yang, E. Y. Zhao, T. Sun, X. B. Zhang, S. Wang, X. Q. Yu, J. M. Yan, Q. Jiang, *Chem* **2019**, *5*, 168–179.
- [137] Z. Tong, R. Yang, S. Wu, D. Shen, T. Jiao, K. Zhang, W. Zhang, C. S. Lee, *J. Mater. Chem. A* **2019**, *7*, 19581–19588.
- [138] S. Chong, Y. Wu, S. Guo, Y. Liu, G. Cao, *Energy Storage Mater.* **2019**, *22*, 120–127.
- [139] J. Wang, L. Fan, Z. Liu, S. Chen, Q. Zhang, L. Wang, H. Yang, X. Yu, B. Lu, *ACS Nano* **2019**, *13*, 3703–3713.
- [140] T. Deng, X. Fan, J. Chen, L. Chen, C. Luo, X. Zhou, J. Yang, S. Zheng, C. Wang, *Adv. Funct. Mater.* **2018**, *28*, 1800219.
- [141] K. Moyer, J. Donohue, N. Ramanna, A. P. Cohn, N. Muralidharan, J. Eaves, C. L. Pint, *Nanoscale* **2018**, *10*, 13335–13342.

Manuscript received: January 30, 2021
Revised manuscript received: March 11, 2021
Accepted manuscript online: March 11, 2021
Version of record online: March 30, 2021